Explor. Mining Geol., Vol. 8, Nos. 1 and 2, pp. 21–42, 1999

0964-1823/98 $17.00 + .00

BRAZIL

The Vazante Zinc Mine, Minas Gerais, Brazil: Constraints on Willemitic Mineralization and Fluid Evolution

LENA VIRGÍNIA SOARES MONTEIRO, JORGE SILVA BETTENCOURT
Instituto de Geociências, Universidade de São Paulo
São Paulo, SP, Brazil

BARUCH SPIRO
Natural Environment Research Council, Isotope Geosciences Laboratory
Keyworth, Nottingham NG 125GG, United Kingdom

RODNEI GRAÇA and TOLENTINO FLÁVIO DE OLIVEIRA
Companhia Mineira de Metais
Vazante, Minas Gerais, Brazil

Received October 7, 1998; approved November 1, 1999.

Abstract — The Vazante Mine is located in the Vazante District, the largest zinc district in Brazil. The Vazante deposit consists dominantly of an unusual willemitic ore. Small sulfide bodies are tectonically imbricated with the willemitic ore, within the Vazante shear zone. Structural styles of deformation and petrographic and isotopic evidence indicate that willemitic mineralization and deformation occurred synchronously during the Neo-Proterozoic. Various generations of hydrothermal veins and hydraulic breccias may pre-date, accompany and overprint the mineralization. Ore-formation temperatures are deduced from stable isotope geothermometry and mineral chemistry of both sulfide bodies and willemitic ore. Temperatures during the main stage of mineralization range from 206°C to 294°C (willemitic ore) and 317°C (sulfides), and reflect the prevailing metamorphic conditions within the shear zone. The fluid from which the gangue minerals of the sulfide bodies precipitated (at 250°C) had an oxygen isotopic average value of $\delta^{18}O = +19.4‰$. This value appears to reflect the interaction of metamorphic fluid with the carbonate rocks of the Vazante formation. At 250°C, the fluid in equilibrium with the vein mineral phases and willemitic ore assemblage exhibits a uniform oxygen isotopic composition, with an average value of $\delta^{18}O = +11.5‰$. The positive linear covariance of $\delta^{18}O$ and $\delta^{13}C$ ratios of the carbonates is most likely due to the mixing of metamorphic and meteoric fluids. The $\delta^{34}S$ values of sulfides indicate a direct crustal origin for the sulfur. It is suggested that the sulfur is largely derived from pre-existing sulfide bodies and has been transported by metamorphic fluids. The willemitic ore may have originated from the precipitation of metal in sulfur-poor fluids under oxidized conditions, within the Vazante shear zone.

Introduction

The Vazante zinc mine is located in the northwest part of the Minas Gerais state, Brazil (Fig. 1). It is the largest zinc mine in Brazil. The mine has been worked since 1968. Production has been from both an open pit and an underground mine, started in 1969 and 1983, respectively. To December 1997, approximately 10.3 Mt of ore grading 20 wt% Zn have been mined and a total of 2 066 800 t of Zn metal have been recovered. The current production rate is 100 000 tpy of Zn, 5000 tpy of Zn oxide and 75 tpy of cadmium. The measured reserves to a depth of 250 m are estimated at 8.9 Mt with an average grade of 22 wt% Zn.

Willemitic ore is the main base-metal ore type. It is composed of willemite, quartz, dolomite, ankerite, siderite, hematite, chlorite, barite, franklinite, and zincite. This association is unusual in relation to base-metal deposits, but is quite similar to classic willemite and franklinite occurrences such as the Sterling Hill and Franklin Furnace deposits (U.S.A.) (Frondel and Baum, 1974; Johnson et al., 1990). It is also similar to the mineral assemblages of the Bob Zinc and Star Zinc deposits in Zambia (Sweeney et al., 1991).

The lack of reliable and widespread geological data has made the genesis of the Vazante deposit controversial. It is clearly different from the other deposits that occur in the same ore-field, within the Vazante-Unaí region, such as the Morro Agudo deposit. This deposit is a sulfide-dominant zinc-ore and represents a SEDEX-type deposit (Misi et al., 1996; Freitas-Silva and Dardenne, 1997) or Irish-type deposit (Hitzman et al., 1995).

The current genetic model for the Vazante willemitic ore suggests that it was formed by supergene processes

(Amaral, 1968; Rigobello et al., 1988) or hydrothermal epigenetic processes closely linked to the development of the Vazante Shear Zone (Pinho, 1990; Pinho et al., 1989, 1990; Monteiro, 1997; Monteiro et al., 1996). However, due to the unusual mineral assemblage, and significant differences from the other carbonate-hosted zinc-lead deposits worldwide, it is difficult to draw analogies with other Zn-Pb deposits.

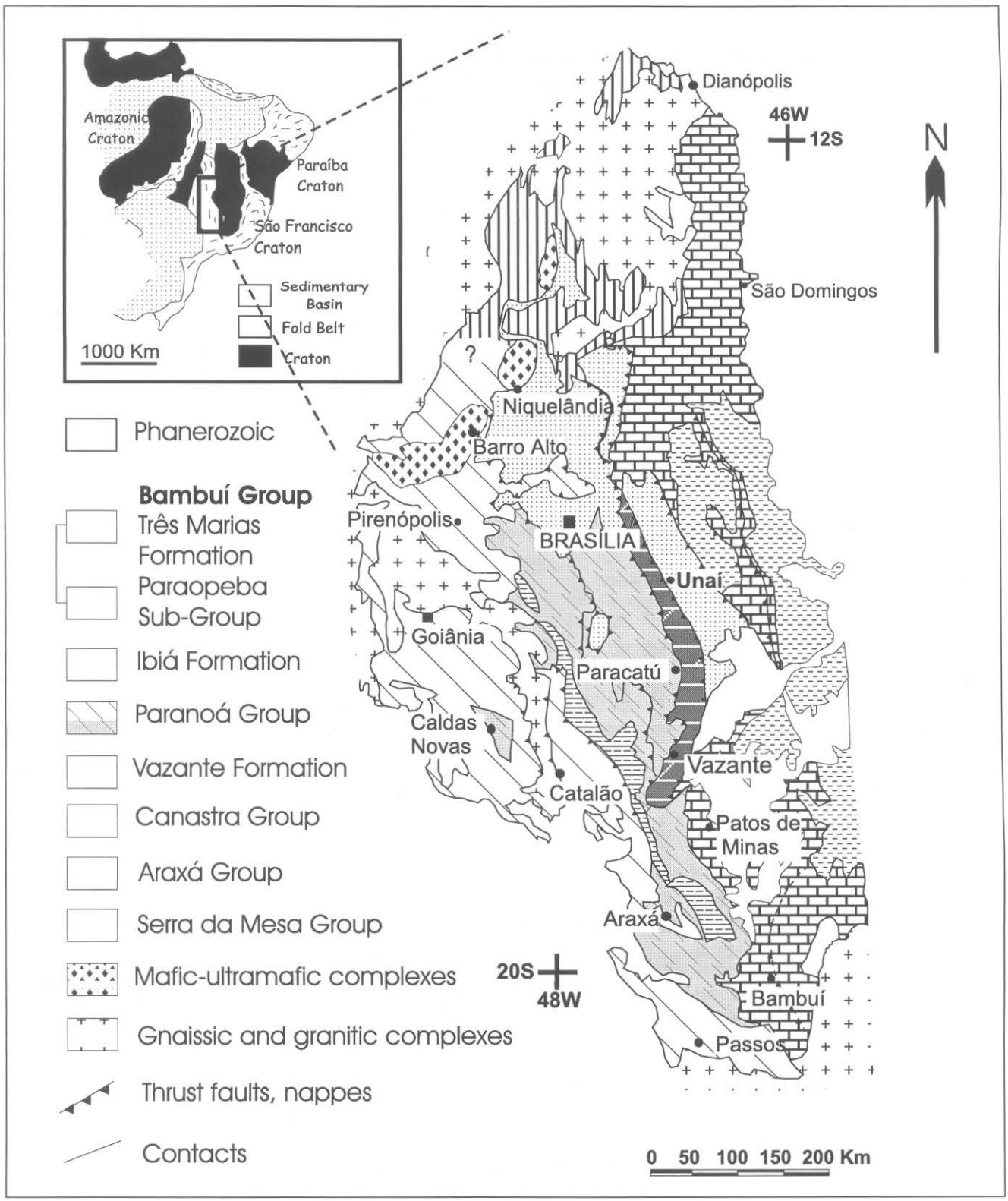

Fig. 1. Location map and geotectonic setting of the Vazante formation, in the Brasília Fold Belt (after Schobbenhaus et al., 1981 and Fuck et al., 1993).

The purpose of this paper is to discuss the geological attributes of the Vazante primary zinc deposit and use these as a basis for the development of a genetic model for this uncommon type of mineralization.

Regional Geologic Setting

The Vazante Mine is located in the eastern part of the Brasília Fold Belt (Almeida, 1967) which is one of the longest continuous features related to the Brasiliano Orogeny (~600 Ma) extending for 800 km over a width of 300 km along the São Francisco Craton. The fold belt represents an unstable crustal block that was subsequently affected by successive stages of reactivation of ancient (Archean) continental rift structures (Marini et al., 1981).

The Brasília Fold Belt displays sequences of rocks thrust to the east, with increasing deformation and metamorphism to the west (Marini et al. 1981). During the Brasiliano Orogeny, the region (Fig. 1) was affected by a regional compressive stress regime related to the closure of the basins. This closure was responsible for nappe structure systems and subsequent deformation of the Vazante formation, the host of the zinc mineralization (Almeida, 1993).

In addition, the transpressive tectonic regime permitted the development of extensive brittle-ductile shear zones with sinistral transcurrent displacement (Valente, 1993). This can be seen in the Vazante Shear Zone, which is the main structural feature of the studied area.

The Vazante Formation: Geological Attributes

The zinc mineralization occurs in the metasedimentary rocks of the Vazante formation (Dardenne, 1978, 1979), which is part of the Brasília fold belt. According to Fuck (1994) and Rigobello et al. (1988), the Vazante formation (Fig. 2) encompasses reef complexes (Upper and Middle facies of Pamplona member) and lateral variations from offshore to tidal flat facies (Lower facies of Pamplona member and Morro do Pinheiro member).

Conophyton stromatolites in the Vazante formation (Dardenne 1978, 1979; Da Rocha Araújo et al. 1992; Freitas-Silva and Dardenne, 1997), indicate that it is older than the Bambuí Group (950 Ma to 650 Ma; Babinski, 1993), which is the platformal cover of the São Francisco craton. This type of stromatolites indicates relative age intervals of 1650 Ma to 950 Ma (*Conophyton Cylindricus Maslov*,

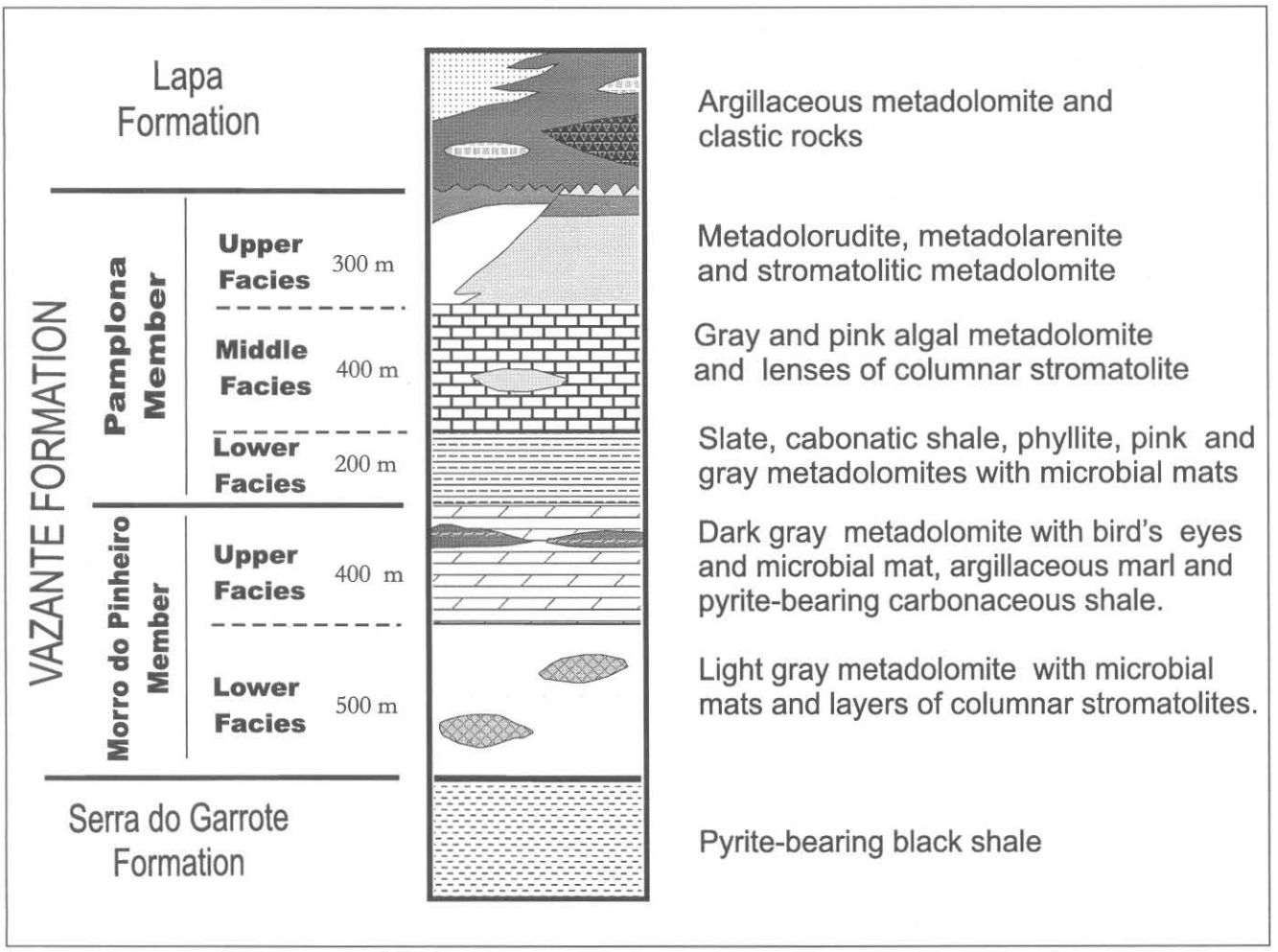

Fig. 2. Stratigraphic column of the Vazante units in the Vazante mining area (Rigobello et al., 1988).

Moeri, 1972) and 1350 Ma to 950 Ma (*Conophyton metula Kirichenko*, Cloud and Dardenne, 1973) while in the Bambuí Group only *Gymnosolen* stromatolites (950 Ma to 650 Ma) are reported (Marchese, 1974).

$^{207}Pb/^{206}Pb$ analyses of galena and Rb-Sr whole rock isochrons for shales from the Vazante formation yield ages which agree well with those of the Bambuí Group, varying between 570 Ma and 750 Ma (Amaral, 1966, 1968; Amaral and Kawashita, 1967; Cassedane and Lasserre, 1969; Iyer, 1984; Iyer et al., 1992, 1993; Misi et al., 1997), as summarized in Table 1. However, these ages may only represent the last closing of the isotopic systems during the Brasiliano metamorphic event that affected both sequences.

Iyer (1984) and Iyer et al. (1992, 1993) reported marked differences between galena from the Bambuí Group and from the Vazante region. The first contains markedly radiogenic J-type lead, whereas the galena from Vazante is less radiogenic and displays an isotopic zonation. These authors considered all the galena samples in their studies to be from Mississippi Valley-type deposits.

Freitas-Silva (1996), Freitas-Silva and Dardenne (1997), Dardenne and Freitas-Silva (1998) consider that the lead isotope data indicate different mineralizing processes for the galena from the Bambuí Group and Vazante region. According to these authors, additional analyses of galena from the Vazante formation and reinterpretation of available data yielded $^{207}Pb/^{206}Pb$ ages of 1200 Ma (Table 1). This age could represent the timing of the lead separation from the basin itself, or the mineralization age of the Morro Agudo deposit, which is considered diagenetic and similar to an Irish-type deposit (Hitzman et al., 1995; Dardenne and Freitas-Silva, 1998). An approximate remobilization age of 680 Ma (Brasiliano Orogeny) is also estimated from the galena of the Morro Agudo and Vazante deposits (Freitas-Silva and Dardenne, 1997).

Vazante Mine Geology

The bulk of the mineralization is associated with two distinct facies of the Vazante formation (Fig. 2): the Morro do Pinheiro member upper facies (footwall sequence) and the overlying Pamplona member lower facies (Rigobello et al., 1988). Their stratigraphic relationships are shown in Figures 2 and 3.

The rocks of these units consist of dolomite, shale, marl, and pelites, which were metamorphosed to greenschist facies. The units form a homoclinal sequence, which generally

Table 1. Geochronological data for the Vazante Formation and for the Bambuí Group

Localization	Sample	Method	Age (Ma)	Interpretation	Model
Vazante Formation					
Vazante deposit (1)	Shale	Rb/Sr	600 ± 50	Deposition age	
Vazante deposit (2)	Galena	Pb/Pb	600 ± 30	Lead separation	Russel and Farquhar (1960)
Vazante deposit (3)	Galena	Pb/Pb	740 ± 40	Type-B galena	Holmes-Houtermans; Holmes (1946); and Houtermans (1946)
Vazante/Paracatú region (4, 5, 6)	Galena	Pb/Pb	650 ± 50	Mineralization age	Single Stage model III (Cumming and Richards, 1975)
Morro Agudo deposit (7)	Primary galena	Pb/Pb	1200	Lead separation or mineralization age	Plumbotectonic Model (Doe and Zartman, 1979; Zartman and Doe, 1981)
			680	Remobilization age	
Vazante deposit (7)	Remobilized galena	Pb/Pb	680	Remobilization age	Plumbotectonic Model
Morro Agudo deposit (8)	Galena	Pb/Pb	1800	Lead separation from basement rocks.	Two-stage model (Stacey and Kramers, 1975)
			650	Mineralization age	
Bambuí Group					
São Francisco (9)	Shale	K/Ar	576 ± 12 to 662 ± 18	(minimum age) metamorphism	
São Francisco (10)	Limestone and shales	K/Ar	582 ± 12 to 607 ± 15	(minimum age) metamorphism	
Montalvânia (11)	Limestone	$^{87}Sr/^{86}Sr$	680 – 570	Deposition age $^{87}Sr/^{86}Sr = 0.7077$	
Montalvânia (12, 13)	Limestone	$^{87}Sr/^{86}Sr$	600	Deposition age $^{87}Sr/^{86}Sr = 0.70745$	
Patos de Minas (3)	Galena	Pb/Pb	605 ± 100	Type-J galena	Holmes – Houtermans
Tiros, Pains, Sete Lagoas, Januária e Montalvânia (4, 5, 6)	Galena	Pb/Pb	1800	Lead separation from basement rocks	Two-stage model (Stacey and Kramers, 1975)
			650	Mineralization age	
Januária, Arcos and Pains (14)	Carbonate rocks	Pb/Pb	2100	Lead separation	Two stage model (Stacey and Kramers, 1975)
			500 – 550	Incorporation of radiogenic lead	
			686 ± 69	Minimum depositional age	

References: (1) Amaral and Kawashita (1967); (2) Amaral (1968); (3) Cassedane and Lasserre (1969) ; (4) Couto et al. (1981); (5) Iyer (1984); (6) Iyer et al. (1992, 1993); (7) Freitas-Silva and Dardenne (1997); (8) Misi et al. (1997); (9) Thomaz Filho and Bonhome (1979); (10) Thomaz Filho and Lima (1981); (11) Kawashita et al. (1987); (12) Kawashita et al. (1993); (13) Chang et al. (1993); (14) Babinski (1993).

trends N50°E and dips 15°NW. Sedimentary and diagenetic structures are well preserved. However, a planar fabric, the S_1 foliation, which is related to a regionally pervasive ductile deformation, is sub-parallel to the microbial-mat lamination of the metadolomites and to the stratification of metapelites.

The Morro do Pinheiro member (upper facies) includes gray metadolomites, carbonaceous black shale, and marl. The metadolomites consist of mudstone with less than 10% intraclasts and pellets. The micritic portions of these metadolomites contain stromatactis-type structures with acicular (or fibrous) spar and mosaic dolomite fillings. Microstalactitic cement and associated internal sediments are present at the bottom of this geopetal structure. Breccia layers within the Morro do Pinheiro member are characterized by fibrous-radiaxial dolomitic cement and fragments of dismicrite, including microstalactitic cement and portions of internal sediments. Their textures indicate local environmental variations from low-energy (inter/subtidal flat) to high-energy settings, which permitted sediment break-up and later marine cementation.

The metadolomite contains pyrite-bearing carbonaceous shale intercalation related to microbial mats. The microbial-mat acted as an ecological membrane, and may have caused an increase of H_2S, and physico-chemical environmental changes, thus favoring the establishment of a microeuxinic environment in the inter/subtidal setting.

The Lower facies of the Pamplona member is composed of either terrigenous metasediments or light gray to pink metadolomites with interbedded slate and sericite phyllite. The gray metadolomite has microbial mats, tepees, pellets, intraclasts, and intraformational breccia layers. It also displays neomorphically-derived microspar or pseudospar textures. Sub-angular to angular detrital quartz and microcline grains indicate mineralogical and textural immaturity. Authigenic minerals are biterminated quartz, feldspar, phlogopite, and, more rarely, pyrite. Voids were filled by dog-tooth and drusy mosaic calcite cement associated with quartz or chert. Dolomitization is selective and/or associated with stylolitic surfaces, which contain iron oxides. Pink metadolomite contains ooids, exhibits silicification parallel to stratification, and has irregular crusts, which are similar to the trapping of insoluble material in calcrete. These features are typical of an inter-supra-tidal setting, with local evaporitic conditions and periods of sub-aerial exposure.

Minor magmatism associated with this sequence is represented by small bodies of metabasic rocks tectonically

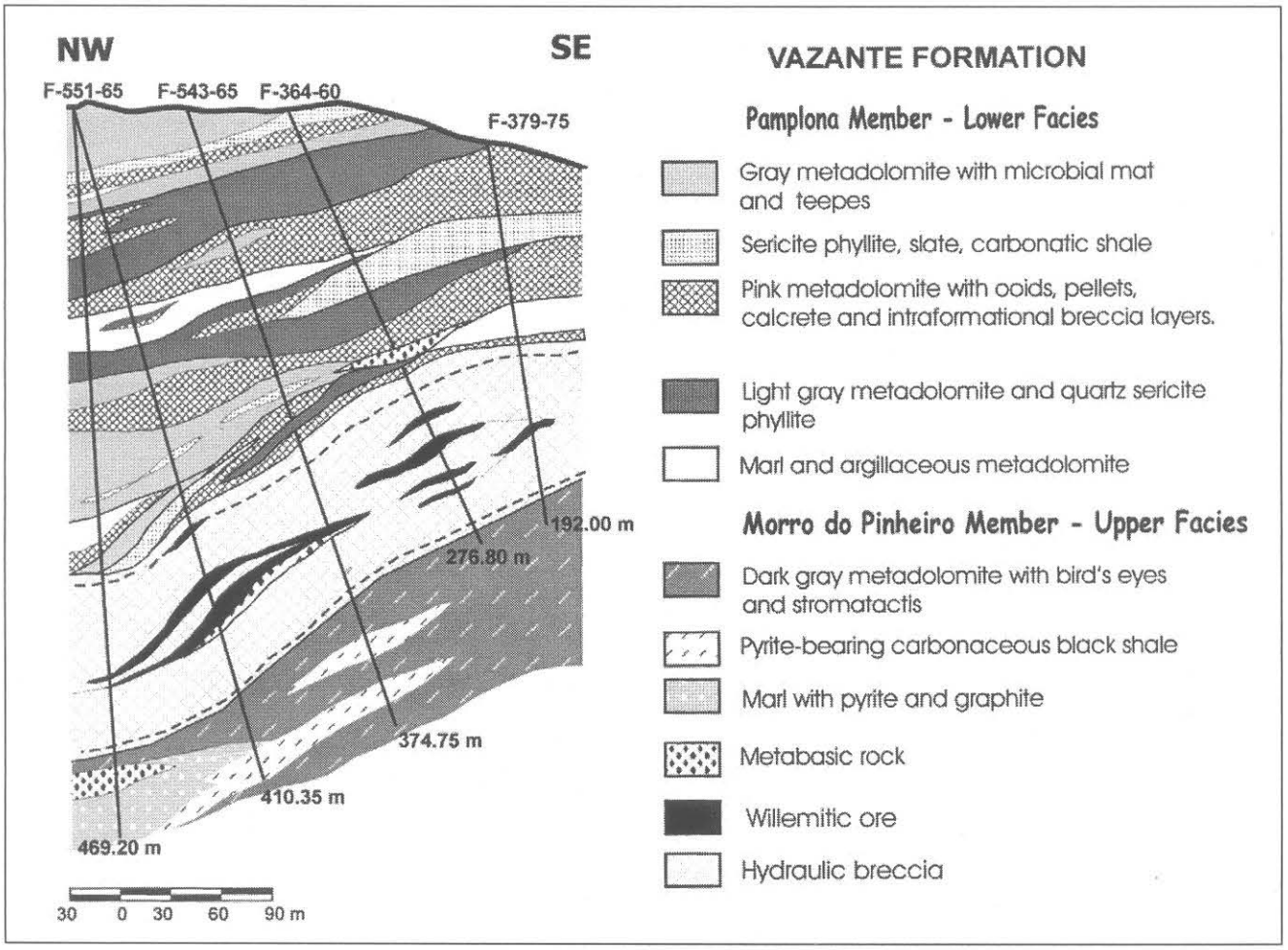

Fig. 3. Cross-section of the Vazante ore zone showing the spatial relationship between host sequence, willemitic ore and the Vazante shear zone. The Vazante shear zone is indicated by the dashed lines.

imbricated with sedimentary layers of the Morro do Pinheiro and Pamplona members, and with willemitic ore along shear zones. This rock type was initially interpreted to be diabase dikes of the Cretaceous age (Rigobello et al., 1988). However, their metamorphic mineral assemblages and mylonitic fabrics are features which indicate that this magmatic unit was affected by the Brasiliano deformation event. These features are not recorded in Brazilian Cretaceous rocks.

The metabasic rock exhibits a relict sub-ophitic igneous texture and consists of the primary minerals plagioclase, pyroxene, ilmenite, and a greenschist facies metamorphic assemblage of chlorite, clinozoizite, epidote, talc, sericite,

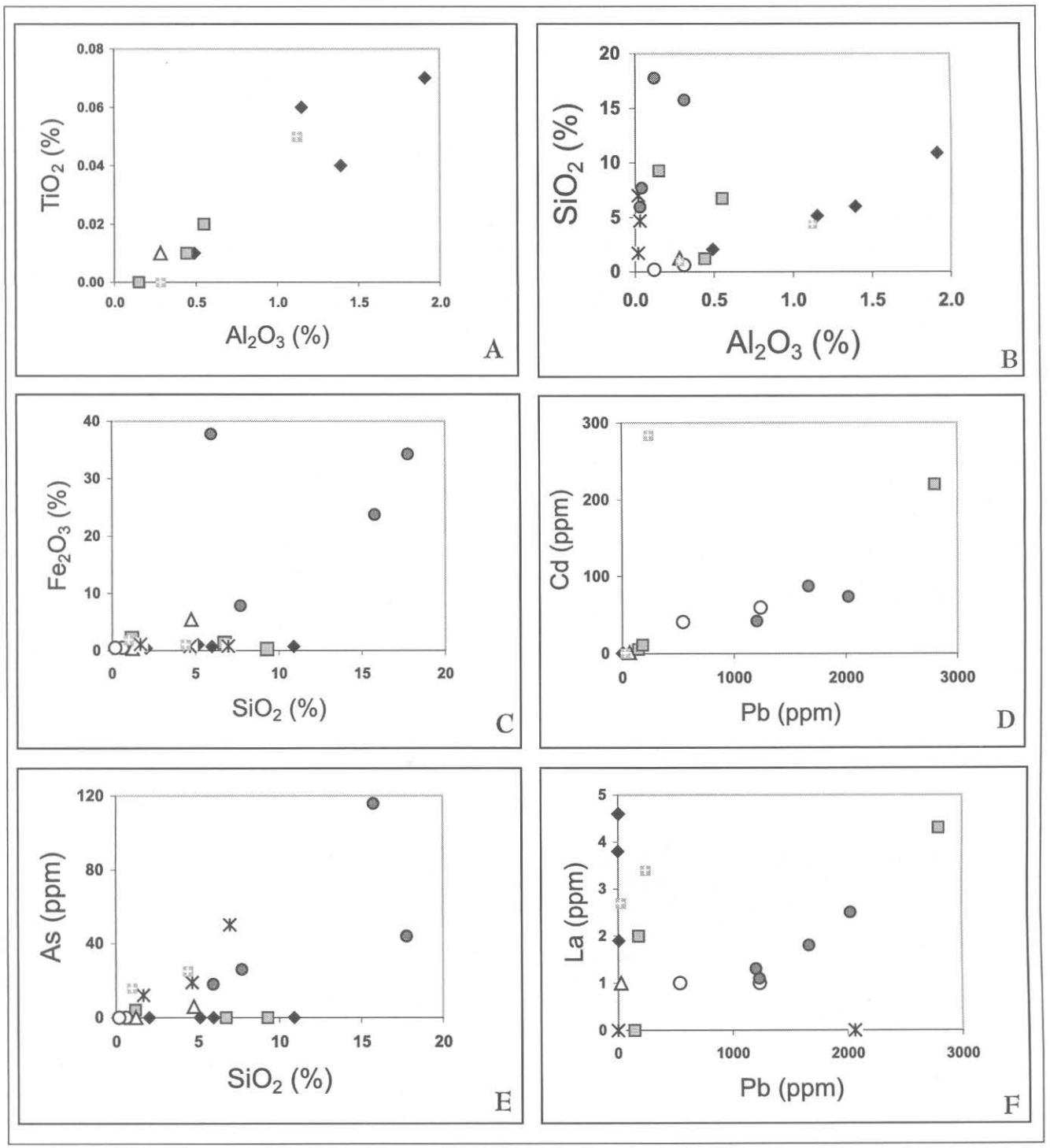

Fig. 4. Bivariate diagrams showing apparent positive correlation between: A — Al_2O_3 and TiO_2 in unaltered, hydrothermally altered and bleached metadolomites. B — SiO_2 and Al_2O_3 in unaltered and bleached metadolomites. C — Fe_2O_3 and SiO_2 in the willemitic ore samples. D — Pb and Cd in altered metadolomites and willemitic ore. E — SiO_2 and As in bleached metadolomite, sulfide orebodies and willemitic ore. F — Pb and La in willemitic-ore samples. Symbols as in Figure 6.

quartz, rutile, leucoxene, and apatite. Biotite remnants indicate the early introduction of potassium. Fe-chlorite, hematite and dolomite formation, associated with S-C structures, overprints the biotite, accompanying the total destruction of igneous textures and minerals.

Hydrothermal Alteration Related to Vazante Shear Zone

The Vazante shear zone trends N50°E, plunges 60°NW and displays a dominant sinistral transcurrent displacement (Pinho, 1990; Pinho et al., 1989, 1990). This is characterized by complex zones of irregular anastomosing geometry and by a structural pattern of intersections between C foliation planes and C, R, R', P, and T Riedel-type shear fractures (Riedel, 1929). The brittle-ductile S_n represents a mylonitic S-C foliation and brittle S_{n+1} and S_{n+2} structures correspond to oblique foliations, exhibiting patterns similar to flower structures and brittle fractures, respectively.

Within the shear zone, hydrothermal alteration is largely fracture controlled, producing a complex zone of net veined breccia (Laznicka, 1989). This is the result of the replacement of unaltered rocks by Fe-bearing minerals, such as siderite, ankerite, hematite, jasper, and chlorite, as well as dolomite, quartz, and chert.

Veins and hydraulic breccias of varying ages are subparallel or perpendicular to the original metadolomite layering, in the plane of the principal displacement shear, (C), and in the secondary synthetic, (P), and T-type Riedel tension shears (extension gash veins) that developed in a consistent system of brittle-ductile simple shear.

Siderite, ankerite, quartz, and jasper commonly predate or accompany the mineralization. Hematite and chlorite veins also cut and replace the willemitic ore. Dolomite is a common mineral phase in all generations of veins and also forms the matrix of cataclastic breccias and veins that postdate the ore formation. The veins display successive crustiform layering, indicating that growth occurred by progressive infilling of open fractures by different precipitates. A foliated texture due to mylonitization also occurs in some veins.

There is little evidence of pervasive alteration within the fault zone, but it is better developed below the mineralized zone, in the Morro do Pinheiro dolostone. The color of the dolostone changes from dark gray to pink, due to ankerite and siderite formation along the mylonitic planes. Initially, this process produces a banded fabric that increases progressively to a massive pink alteration. Chert and hematite occur in cataclastic structures, and gahnite veinlets are common.

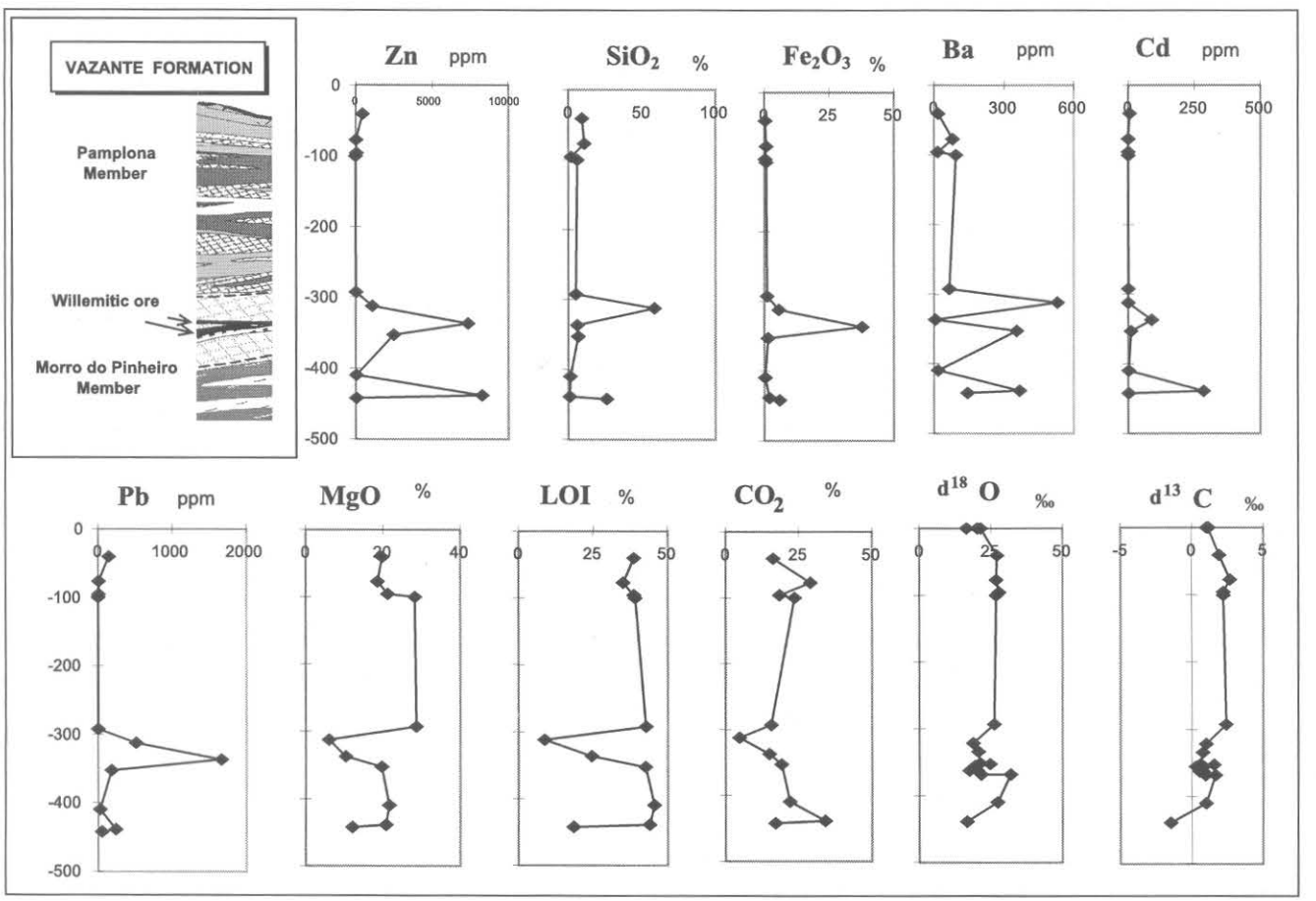

Fig. 5. Profiles of geochemical, oxygen, and carbon isotope compositions of metadolomites relative to stratigraphic position along drill hole F-551-65°.

The Pamplona dolostone over the deposit is strongly brecciated and cut by hydrothermal veins. Silicification, in the form of chert and microcrystalline quartz, occurs preferentially along mylonitic planes, fractures or, more rarely, as a secondary vug infilling. The original microspar or pseudospar texture is replaced by non-planar dolomite (Sibley and Gregg, 1987), which is characterized by closely packed anhedral crystals with undulatory extinction under crossed polarized light.

The Pamplona slates contain chlorite, phlogopite, calcite, hematite, chert, and dolomite along the mylonitic foliation. Silicification occurs as chert and quartz veins often formed within fabric-controlled, conjugate fractures and mylonitic penetrative foliation. Prominent structures indicative of tectonic deformation such as stretched detritic-quartz, drag folds, stylobreccias, and chalcedony-filled pressure shadows on pyrite are common in the slates.

The metadolomites are bleached and metasomatically altered along the contact with metabasic rocks and exhibit calcite fillings in fractures parallel to the mylonitic C fabric. A metasomatic assemblage of Fe-chlorite, serpentine, chert, and saddle dolomite is recognized within this zone.

The metabasic rock has been altered to chlorite and chrysotile that are associated with S_{n+1} brittle-ductile foliation. Dolomite formation and replacing of ilmenite by leucoxene, rutile, and hematite are related to S_{n+2} brittle structures. These alterations result in the total destruction of igneous textures and minerals.

Strong enrichment of Zn and Pb in all lithotypes present in the shear zone is the most pervasive chemical modification. Unaltered rocks have correlations of SiO_2, Fe_2O_3, MnO, Sc, W, Zr, Y, Th, V, Ba, Sr, Ag, Cu, Co, Ni, and REE with Al_2O_3, K_2O and TiO_2 (Figs. 4a and 4b). A detrital origin, related to clay minerals, is suggested to explain this correlation. In altered rocks, this pattern is absent (Fig 4b).

Within the willemitic ore zone, the rocks display an apparent positive correlation between SiO_2, Fe_2O_3, Zn, Pb, Ba, Cu, and Cd (Figs. 4c, 4d and 5) while the small sulfide bodies exhibit an apparent correlation between Zn, Ba, Cu, Cd (Fig. 5). The enrichment of SiO_2 (Fig. 4b) and Fe_2O_3 (Figs. 4c and 6), in altered and mineralized rocks, could indicate a hydrothermal source. A hydrothermal process could also be responsible for the enrichment of As, Sb, W, V, and LREE (Figs. 4e and 4f), which are associated particularly with hematite-rich willemite ore, as indicated by the increase of La/Sm ratios in this ore type, as follows: 5.45 (unaltered rocks); 5.52 (altered rocks); 6.90 (bleached dolomite); 9.25 (willemitic ore with up to 10% hematite) and 13 (willemitic ore with up to 30% hematite).

Zinc Ore

Willemitic ore is the main ore type in the Vazante deposit. It occurs as pods that are controlled by intersections of C, P, R, and R' shear planes, and veins related to T-type shear fractures. The willemitic pods are tectonically imbricated with small sulfide orebodies, metabasites, and brecciated metadolomites. The sulfide orebodies are off-set by normal and reverse faults and also cut by late hydrothermal veins, which causes complex relationships between orebodies and the host sequence.

The small sulfide orebodies occur as lense-shaped irregular bodies with a well-developed mylonitic fabric, elongated parallel to C shear planes (Fig.7), or are localized within late-vein fillings. These orebodies are composed mainly of colorless iron-poor sphalerite (80% to 95%), with

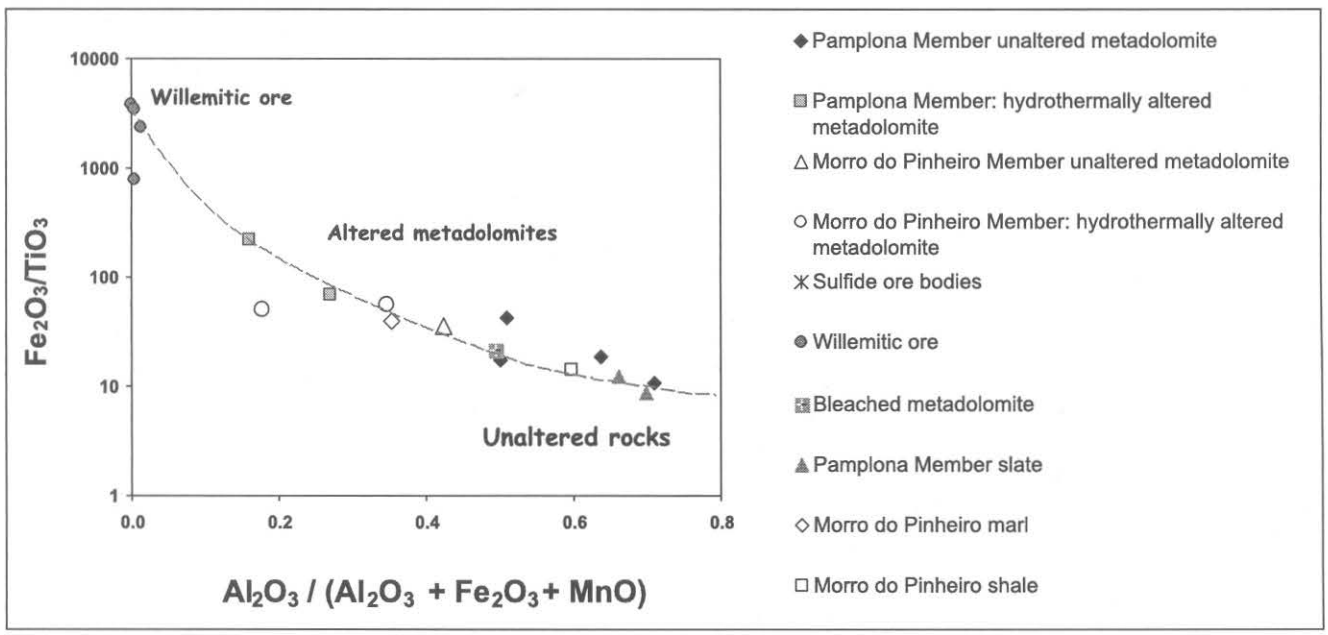

Fig. 6. Plot of $Al_2O_3/(Al_2O_3 + Fe_2O_3 + MnO)$ versus Fe_2O_3/TiO_2 for Vazante samples (n = 25), showing a hydrothermal contribution of Fe_2O_3 in altered and mineralized rocks (after Boström, 1973 and Peter and Goodfellow, 1996).

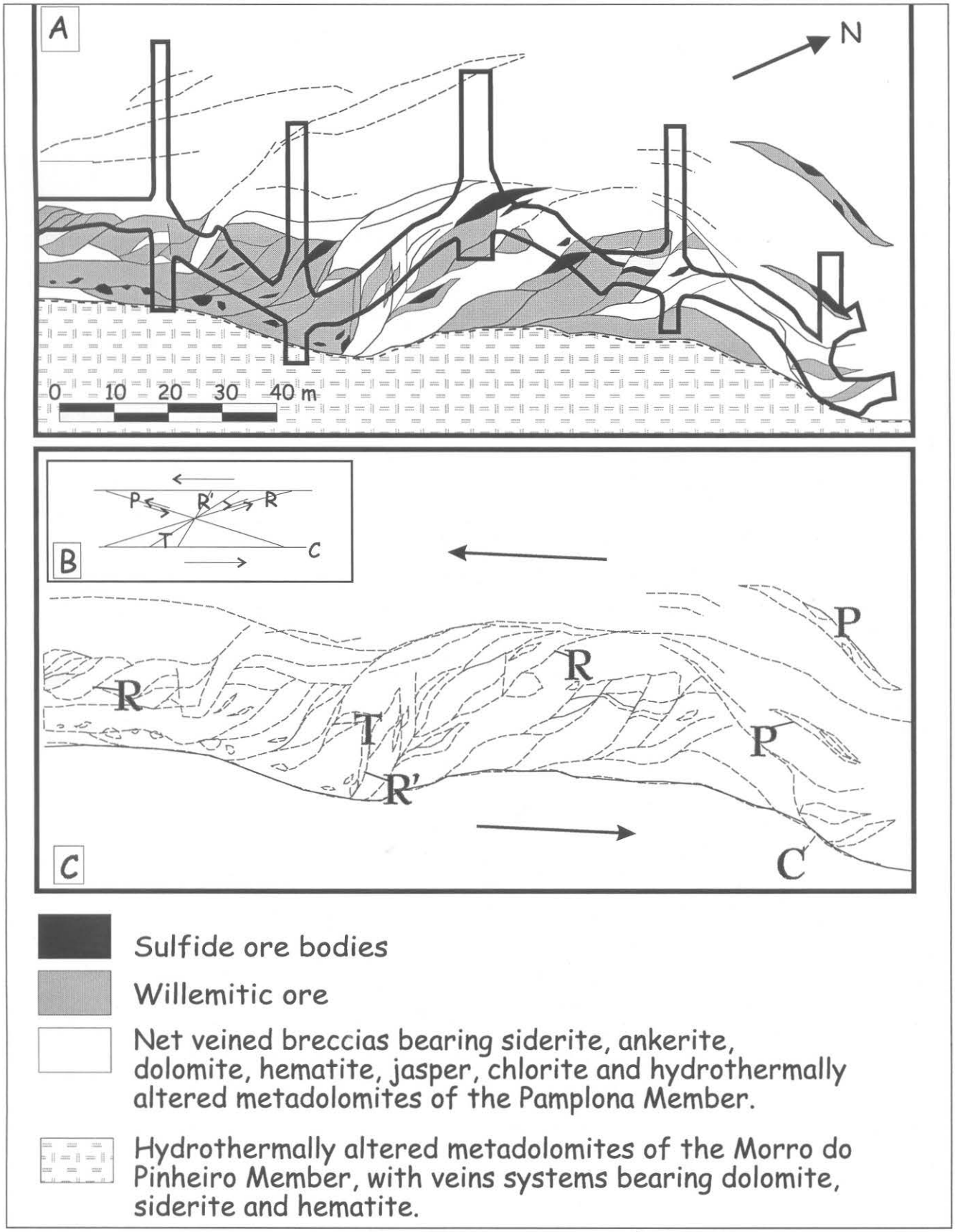

Fig. 7. Geology of the 500 ft level, between GV500/SW100 and GV500/NW050 area, showing: A — the morphology and distribution of the orebodies. B — the theoretic model for relationships between Riedel structures (C, P, R, R', and T). C — the structural controls of sulfide and willemitic ore, related to the Vazante shear zone (compiled and modified after Cia. Mineira de Metais files).

round inclusions of galena (5% to 20%). The sphalerite contains small inclusions of hematite, quartz, and dolomite as well, all strongly deformed and stretched along the mylonitic foliation (S_n) planes (Table 2).

The brittle-ductile shear zone development is of paramount importance in the mechanical remobilization, recrystallization, and replacement of the sulfides by willemitic assemblages (Figs. 8a and 8b). Willemite formation in the sulfide bodies occurs, initially, along the mylonitic foliation and results in two distinct associations. The first is

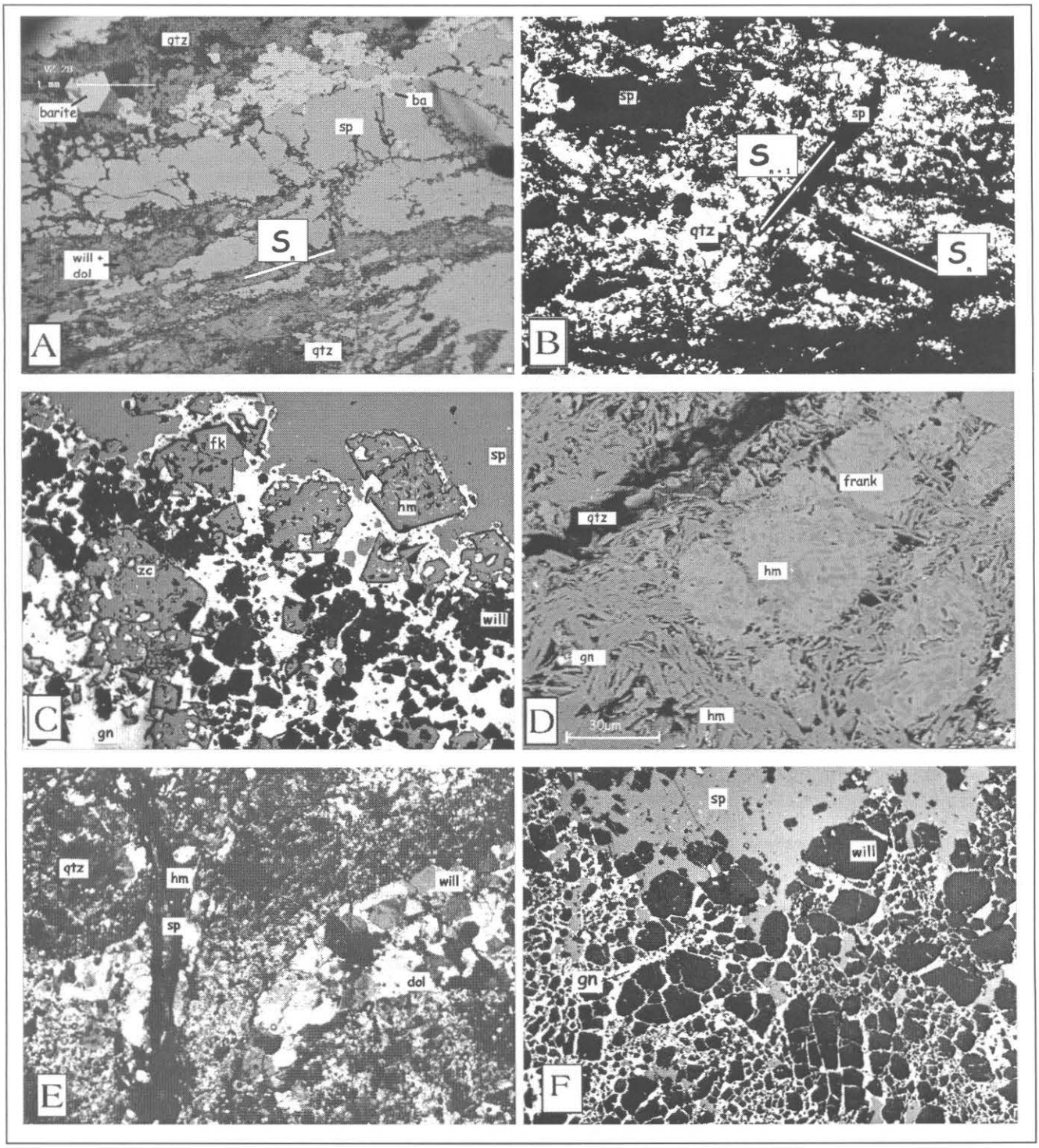

Fig. 8. Photomicrographs of sulfide orebody features. A — SEM image, showing the formation of the willemite, dolomite and quartz alteration assemblage, related to mylonitic fabric (S_n). B — sphalerite remobilization related to S_{n+1} structures (width of field = 5.50 mm; plane — polarized light). C — association of franklinite, sphalerite, willemite, and galena (width of field = 1.39 mm; reflected light). D — hematite and zincite replacing franklinite (SEM image). E — mineral deformation related to brittle-ductile structures, sphalerite remobilization, and formation of granoblastic willemitic aggregates (width of field = 1.39 mm; plane — polarized light). F — fibrous radiate willemite crystals densely fractured and veined by latter galena (width of field = 1.39 mm; reflected light).

willemite, sphalerite, franklinite, and zincite (without quartz) and the second mineral assemblage is willemite with quartz, dolomite, and franklinite (without sphalerite), which occur in pockets. These assemblages suggest the formation of willemite through the following reaction:

$$2\,ZnS + SiO_2 + O_2 = ZnSiO_4 + S_2 \quad \ldots\ldots\ldots (1)$$

sphalerite quartz willemite

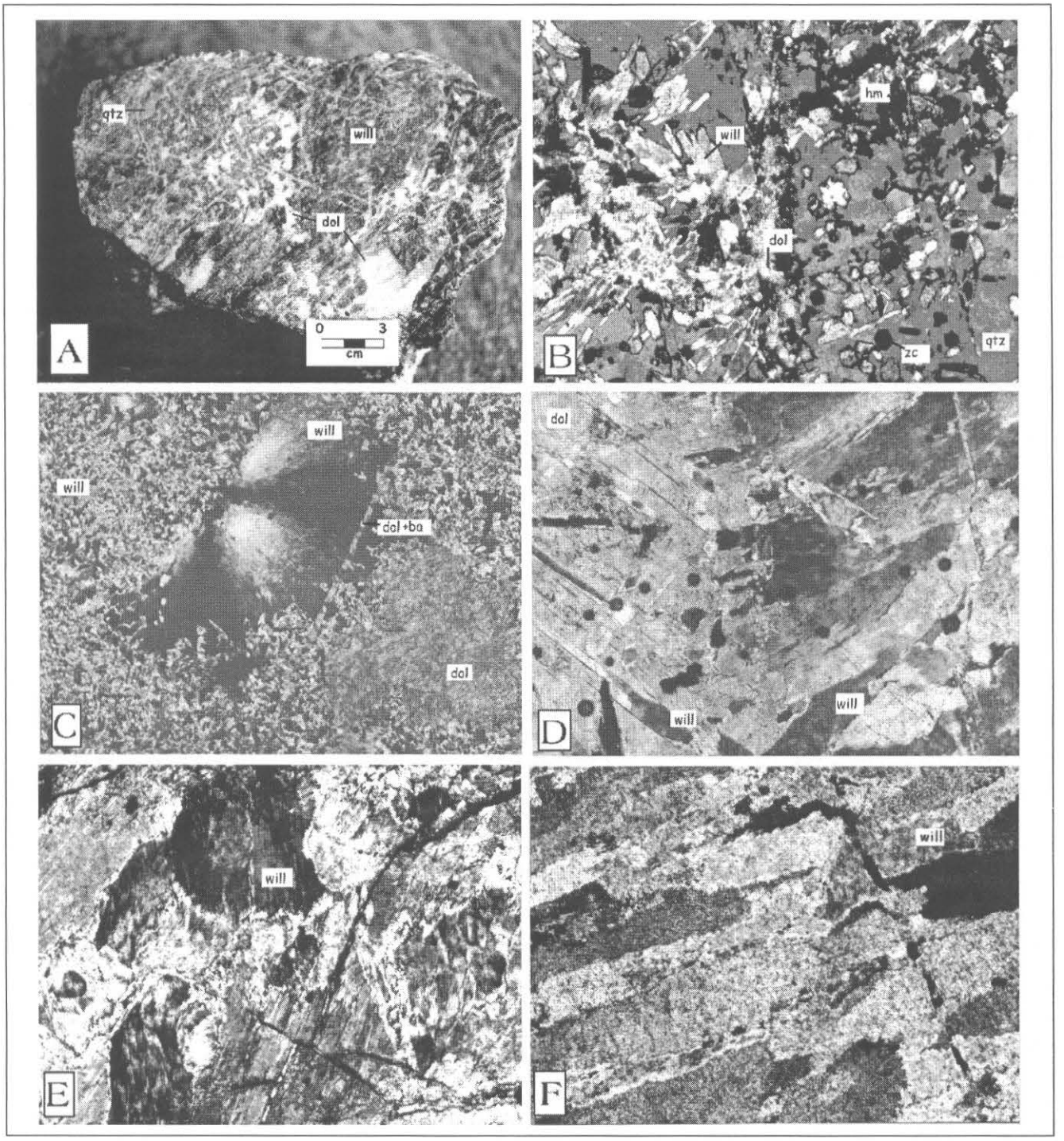

Fig. 9. Photographs of the willemitic ore association. A — hand specimen of the willemitic ore sample. B — photomicrograph of willemitic ore is showing the association of willemite, quartz, dolomite, zincite and hematite. (Width of field = 5.50 mm; crossed polars). C — fibrous, radiate willemite associated to fine willemitic matrix and cloudy dolomite (width of field = 1.39 mm; plane — polarized light). D — relationship between willemite (right) and dolomite (left), showing the willemite crystallization along dolomite cleavage (width of field = 0.70 mm; plane — polarized light). E — willemite deformation related to S_{n+1} brittle-ductile structures (width of field = 0.70 mm; plane — polarized light). F — strong willemite stretching related to S_{n+1} brittle-ductile structures (width of field = 0.70 mm; plane — polarized light).

Table 2. General paragenetic association of the sulfide and willemitic orebodies in relation to brittle-ductile and brittle structures related to Vazante shear zone development

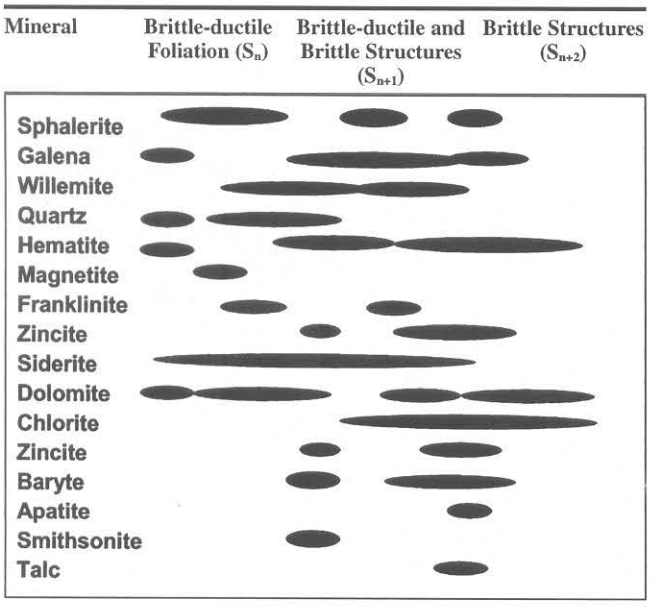

In this mining district, the franklinite (Fig. 8c) is described for the first time in the Vazante deposit. Zn^{2+} substitutes for Fe^{2+} in franklinite. Magnetite intergrowths contain Fe^{2+}, which substitutes to a limited extent, for Zn^{2+}. There is evidence that hematite and zincite have progressively replaced franklinite and magnetite (Fig. 8d). This feature is expressed by the reaction below:

$$ZnFe_2O_4 = Fe_2O_3 + ZnO \quad \ldots\ldots\ldots\ldots (2)$$

franklinite hematite zincite

S_{n+1} structures related to a brittle-ductile regime resulted in the deformation and recrystallization of the willemitic assemblage and in the substitution of fibrous-radiated or prismatic crystals of willemite by granoblastic aggregates of willemite (Fig. 8e). A new generation of willemite is also related to S_{n+1} structures, occurring as fracture or vein filling associated with sphalerite, which indicates the formation of both zinc minerals in the same event.

Willemite crystals are fractured and filled by galena and sphalerite, resulting in a cataclastic texture (Fig. 8f) with brittle character (S_{n+2}).The main ore type of the Vazante mine is willemitic ore (Fig. 9a), which rarely contains sulfides. It is composed of willemite (70% to 50%); dolomite (40% to 10%), quartz (15% to 10%), hematite (10% to 05%), barite (<5%), franklinite (<5%) and zincite (<5%), as summarized in Table 2. Variations of this type of ore include lithotypes with up to 40% hematite and up to 10% chlorite, both of which are concentrated in shear planes and related to the development of the Vazante Shear Zone.

Fibrous-radiated and prismatic willemite is associated with quartz and dolomite (Figs. 9b, 9c, and 9d). It is cut by barite and dolomite veinlets or by veins of very pure willemite associated with franklinite, zincite, and minor sphalerite. The sphalerite in these veins, is almost completely replaced by zincite, suggesting the reaction below, which indicates that fS_2 and fO_2, may have had an important role in the stability of this assemblage.

$$2\,ZnS + O_2 = 2\,ZnO + S_2 \quad \ldots\ldots\ldots\ldots (3)$$

sphalerite zincite

The brittle-ductile deformation of willemitic ore also results in a granoblastic texture and mineral stretching (Figs. 8e and 8f) and is accompanied by the formation of hematite and Zn-rich chlorite. Cataclastic breccia comprises willemitic fragments surrounded by cloudy saddle dolomite and is cut by hematite, chlorite, and dolomite veins. The willemitic ore in tectonic contact with metabasic rocks, displays a different mineral association, characterized by Zn-rich chlorite, which is partially replaced by hematite, talc, and apatite.

Previous studies of the Vazante deposit (Amaral, 1968; Rigobello et al., 1988) indicated a supergene origin for willemite ore. However, petrographic evidence, such as the relationship between willemite formation and the development of microstructures, suggest that the willemitic mineralization and deformation are synchronous episodes related to the Vazante shear zone.

The studies of Essene and Peacor (1987) and Johnson et al. (1990) on the Sterling Hill and Franklin Furnace deposits indicate that under the conditions of 1000°K and 5 kbars, willemite and zincite are stable phases in a restricted range of high fO_2 and low fS_2 values. These redox conditions preclude the precipitation of pyrite and pyrrhotite, and are very different from the conditions commonly met in the majority of base metal deposits.

Petrographic studies of Vazante samples indicate temperature conditions very different from the temperatures of the Sterling Hill and Franklin Furnace studies. At Vazante, the maximum temperature is consistent with greenschist facies conditions. However, the same phase stabilities, associated with high fO_2 and low fS_2, appear to be valid for Vazante mineralizations. This could explain the absence of pyrite in the Vazante deposit. In addition, the replacement of sphalerite by willemite or zincite could be related to variations of the fO_2/fS_2 ratio during fluid evolution.

Analytical Techniques

Sampling at Vazante was undertaken in the underground mine and from drill cores. SEM analyses were carried out at the Laboratório de Caracterização Tecnológica, of the Departamento de Engenharia de Minas-POLI, Universidade de São Paulo, using a Leica Stereoscan 440/quantimet 600S, equipped with a back-scattering electron detector coupled to a microanalysis system with spectrometry by R-X fluorescence and EDS detector. Microprobe analyses were done on a CAMECA 50 instrument at the Universi-

dade de Brasília and a Jeol, JXA 8600 SuperProbe at the Instituto de Geociências, Universidade de São Paulo.

Whole rock chemical analyses were done at Activation Laboratories Ltd., Canada. The bulk of the major element analyses were completed by ICP-MS, and a suite of trace elements (Cl, Au, As, Br, Co, Cr, Cs, Hf, Hg, Ir, Mo, Rb, Sb, Sc, Se, Ta, Th, U, W, and REE) were done by INAA. Sulfur, total carbon and CO_2 were measured by the LECO method.

Samples were prepared for isotopic analysis by crushing and mechanical separation of individual minerals, or by using a fine dental drill. The analyses were performed at NIGL (NERC Isotope Geosciences Laboratory), of NERC (Natural Environment Research Council) in Keyworth, England.

Oxygen-isotope ratios in silicates and oxides were determined on sample aliquots of approximately 5 mg (quartz) and 10 mg (for other minerals). The oxygen liberation technique of Clayton and Mayeda (1963) was employed. ClF_3 was used as a reagent instead of BrF_5, as described by Borthwick and Harmon (1982). CO_2 isotopic ratios were measured on a CJS Sciences Phoenix 390 mass spectrometer and were reported in the usual δ notation as per mil (‰) relative to the SMOW standard for $^{18}O/^{16}O$ ratios. The $\delta^{18}O_{SMOW}$ results were normalized through NIGL laboratory standard (LQS-Lock Aline Glass Sand) and quested relative to the international standard quartz NBS#28 (African Glass Sand) at a value of 9.63. The determined values of NBS#28 were +9.6‰ ±0.2.

The $^{13}C/^{12}C$ and $^{18}O/^{16}O$ ratios in carbonates samples were determined using the method of McCrea (1950). CO_2 was produced by the reaction of carbonate minerals with H_3PO_4 in high vacuum conditions. CO_2 isotopic ratios were measured on a CJS Sciences Phoenix 390 mass spectrometer and were reported here in the δ notation as per mil (‰) deviations relative to the SMOW standard for $^{18}O/^{16}O$ ratios and to the PDB standard for $^{13}C/^{12}C$ ratios. Eight replicated analyses of a range of unknown samples exhibited an average difference of 0.07‰ for $^{13}C/^{12}C$ ratios and of 0.06‰ for $^{18}O/^{16}O$ ratios.

The $^{34}S/^{32}S$ ratios were determined using the techniques of Rafter (1965) and Sasaki et al. (1979). SO_2 isotopic ratios were measured on a CJS Sciences Phoenix 390 mass spectrometer and were reported in the usual δ notation as per mil (‰) deviations relative to the CDT standard for $^{34}S/^{32}S$ ratios.

Stable Isotopic Constraints

Sulfur Isotopes

The isotopic compositions of sphalerite and galena from sulfide bodies (Table 3) are similar to those from the willemitic ore, and are in the range of $\delta^{34}S_{ZnS}$ = +13.1‰ to +14.4‰ and $\delta^{34}S_{PbS}$ = +11.8‰. However, the diagenetic pyrite of carbonaceous black shale of the footwall sequence (Morro do Pinheiro member) displays a distinctly different isotopic composition ($\delta^{34}S$ = -2.5‰). Diagenetic pyrite could be formed from the reaction of iron oxides and H_2S produced through bacterial sulfate reduction, in an euxinic environment (Donnelly and Crick, 1992). The isotopic composition of biogenic sulfides is determined by kinetic factors, the seawater isotopic composition and by the nature of the involved system, closed or open in relation to SO_4 and H_2S. These factors permit a greater interval of isotopic compositions ($\delta^{34}S$ = -50‰ to +50‰), according to Field and Fifarek (1985), which could be compatible with the isotopic composition of Vazante diagenetic pyrite.

However, the ore sulfides display a distinct isotopic composition in relation to diagenetic pyrite, which precludes the H_2S source through diagenetic pyrite hydration, because this mechanism should result in sulfides with a similar pyrite $\delta^{34}S$ value. Thus, different sulfur sources and formation conditions for diagenetic pyrite and the other sulfides are necessary.

The source of sulfur can only be determined with full knowledge of the isotopic composition of the total sulfur in the system ($\delta^{34}S\Sigma_S$). However, as the sulfur isotopic composition of sulfides is a function of $\delta^{34}S\Sigma_S$, T, pH, and I (ionic strength), the redox condition inferred through the mineral assemblage may inform us about the relation between $\delta^{34}S_{sulfides}$ and $\delta^{34}S\Sigma_S$ (Ohmoto, 1972). The isotopic fractionation results in ^{34}S enrichment in oxidizing species and consequently ^{32}S enrichment in sulfides. Thus, in high fO_2 conditions, as indicated by the stability of mineral associations (willemite, zincite, franklinite, hematite, barite) the relationship $\delta^{34}S_{sulfide} < \delta^{34}S\Sigma_S$ could be valid.

The positive $\delta^{34}S_{ZnS}$ values indicate incompatibility with an igneous sulfur source, with values of $\delta^{34}S\Sigma_S \approx 0$ (Ohmoto and Rye, 1979; Ohmoto, 1986). However, the positive values are consistent with sulfates in equilibrium with Proterozoic seawater ($\delta^{34}S\Sigma_S \approx$ +10‰ to +30‰), and with reduced sulfur

Table 3. Sulfur and oxygen isotope compositions of mineral phases of sulfide orebodies (sphalerite, galena and franklinite) and willemitic ore (willemite, quartz and hematite)

Sample	Mineral	$d^{34}S_{CDT}$ (‰)	$d^{18}O_{SMOW}$ (‰)
Sulfide orebodies			
VZ-01	Sphalerite	+14.40	
F-551-08	Sphalerite	+13.50	
VZ-28	Sphalerite	+13.10	
VZ-29c	Galena	+11.80	
F-466-7	Pyrite	–2.50	
F-551-8	Franklinite		+9.66
Willemitic ore			
VZ-29g	Willemite		+10.95
VZ-29g	Quartz		+18.71
F-551-11	Willemite		+13.00
F-551-I-30	Willemite		+13.80
F-551-I-30	Hematite		+1.16
F- 551-I-35	Willemite		+12.29
F- 551-I-35	Willemite		+13.07
F-551-I-28	Hematite		+0.61
F-551-I-19	Quartz		+22.24
VZ-06	Quartz		+24.04

derived from leaching of basement host rocks or pre-existing sulfides deposits ($\delta^{34}S\Sigma_S \approx +5‰$ to +15‰), which indicate a crustal source for the sulfur (Ohmoto, 1996). The absence of anoxic conditions, restricted to the footwall sequence, may preclude the reduced sulfur formation from sulfate bacterial reduction. Another possibility is that sulfur could originate from the thermochemical sulfate reduction in presence of Fe^{2+}-bearing minerals, which results, according to Ohmoto (1996) in $\delta^{34}S_{sulfides} \approx -8‰$ to +22‰ and/or derived from leaching of pre-existing sulfides. Thus, a hydrothermal sulfur aqueous solution origin (Ohmoto, 1996) could explain the fluid flux into the country rocks, and the dissolution, the assimilation and the transport of sulfur together with metals, and finally remobilized into the shear zone.

Oxygen and Carbon Isotopic Characteristics

The unaltered metadolomites of the Pamplona and the Morro do Pinheiro member yield isotopic compositions in the range of $\delta^{18}O_{SMOW}$ = +27.71‰ to +26.22‰ and $\delta^{13}C$ = +2.68‰ to +2.22‰ and $\delta^{18}O_{SMOW}$ = +27.24‰ and $\delta^{13}C$ = +1.01‰, respectively (Table 4). In $\delta^{18}O$ vs $\delta^{13}C$ space (Fig. 10), the samples cluster into a uniform group. However, the hydrothermally altered metadolomites, which have $\delta^{18}O$ and $\delta^{13}C$ values varying from $\delta^{18}O$ = +27.19‰ to +22.07‰ and $\delta^{13}C$ = +1.93‰ to +0.90‰ (Pamplona member) and $\delta^{18}O$ = +25.60‰ to +24.46‰ and $\delta^{13}C$ = +0.62‰ to +0.53‰ (Morro do Pinheiro), display a co-variance of the oxygen and carbon isotopic values. This feature could reflect an alteration halo, which might be considered an important exploration guide.

The hydrothermal dolomite and siderite of vein systems (Fig. 10) yield average compositions (n = 14) of $\delta^{18}O$ = +19.43‰ and $\delta^{13}C$ = +0.59‰ (Table 4), which could represent a progressive isotopic shift from the unaltered rocks (Fig. 5).

The metadolomites in contact with metabasic rocks display great differences in the isotopic compositions ($\delta^{18}O$ = +21.44‰ to +16.70‰ and $\delta^{13}C$ = -0.22‰ to -1.48‰) relative to unaltered metadolomites. The calcite of this bleached metadolomite, however, has the most distinct $\delta^{13}C$ value (-10.31‰), suggesting a different source of carbon.

The gangue carbonates (siderite and dolomite) associated with sulfide bodies have a $\delta^{18}O$ range of +25.85‰ and +31.85‰, which represent similar or significantly higher val-

Table 4. Carbon and oxygen isotope composition of carbonates from host sequence, hydrothermal veins, sulfide orebodies and willemitic ore

Sample	Description	$\delta^{13}C_{PDB}$(‰)	$\delta^{18}O_{PDB}$(‰)	$\delta^{18}O_{SMOW}$(‰)
Vazante Formation: Lower Facies of Pamplona Member				
F-551-14	Pink metadolomite	+2.43	–4.5	+26.22
F-551-G	Light gray massive metadolomite	+2.68	–4.01	+26.72
F-551-K	Gray metadolomite with microbial mats	+2.22	–3.06	+27.71
F-551-M	Gray parallel-laminated metadolomite	+2.22	–3.97	+26.77
Vazante Formation: Upper Facies of Morro do Pinheiro Member				
F-543-36	Dark gray metadolomite (mudstone)	+1.01	–3.52	+27.24
Vazante Shear Zone				
F-364-11	Hydrothermally altered metadolomite (Pamplona)	+1.93	–3.56	+27.19
F-551-27	Hydrothermally altered metadolomite (Pamplona)	+1.57	–5.99	+24.68
VZ-43	Hydrothermally altered metadolomite (Pamplona)	+0.90	–8.53	+22.07
F-4-2	Hydrothermally altered metadolomite (Morro do Pinheiro)	+0.62	–6.21	+24.46
F-8-2	Hydrothermally altered metadolomite (Morro do Pinheiro)	+0.53	–5.11	+25.6
F-466-3	Bleached metadolomite	–0.22	–9.14	+21.44
F-568-4	Bleached metadolomite	–1.48	–14.44	+16.7
F-466-3	Calcite (associated with bleached metadolomite)	–10.31	+7.58	+23.04
VZ-08	Siderite (tardi-diagenetic, pre-mineralization)	+1.13	–9.22	+21.37
VZ-41b	Dolomite (hydrothermal vein, pre-mineralization)	+0.38	–10.68	+19.85
VZ-41b	Siderite (hydrothermal vein, pre-mineralization)	+0.83	–9.95	+20.6
F-551-19	Dolomite (hydrothermal vein, related to mineralization)	+1.02	–11.64	+18.87
F-551-23	Siderite (hydrothermal vein, related to mineralization)	+0.77	–9.94	+20.61
F-551-26	Siderite (hydrothermal vein, related to mineralization)	+0.63	–9.28	+21.29
F-364-3	Dolomite (hydrothermal vein, related to mineralization)	–1.06	–14.43	+15.98
F-364-3	Siderite (hydrothermal vein, related to mineralization)	+0.76	–9.75	+20.81
F-10-2	Dolomite (hydrothermal vein, related to mineralization)	–0.32	–13.59	+16.85
F-543-10	Dolomite (hydrothermal vein, related to mineralization)	+1.28	–10.82	+19.7
VZ-13	Saddle dolomite (cataclastic breccia, posterior to ore)	–0.12	–11.16	+19.36
VZ-05	Spar dolomite (cockade texture, posterior to ore)	+1.19	–13.99	+16.44
VZ-05	Spar siderite (cockade texture, posterior to ore)	+1.19	–13.99	+16.44
VZ-16	Siderite (cockade texture, posterior to ore)	+1.05	–10.32	+20.22
Sulfide Orebodies				
VZ-28	Hydrothermal dolomite	–5.94	–4.86	+25.85
VZ-28	Hydrothermal siderite	–1.03	+0.68	+31.56
F-551-8	Hydrothermal siderite	+1.66	+0.96	+31.85
F-551-10	Hydrothermal siderite	+0.98	–9.00	+21.58
Willemitic Ore				
F-551-30	Hydrothermal dolomite	+0.57	–13.02	+17.43
F-551-30	Hydrothermal siderite	+0.83	–10.3	+20.24
F-551-28	Hydrothermal dolomite	+0.29	–10.94	+19.58
F-551-28	Hydrothermal siderite	+0.86	–11.13	+19.39

ues than the $\delta^{18}O$ host rock values. The $\delta^{13}C$ values are extremely variable from +1.66‰ to -5.94‰, but are consistently lower than $\delta^{13}C$ values of unaltered host rocks in $\delta^{18}O$-$\delta^{13}C$ space. These isotopic compositions define a distinct covariant trend from that determined for isotopic compositions of carbonates from willemitic ore and altered host rocks (Fig. 10). The calcite from the bleached metadolomite has more affinity with this data than the other hydrothermal carbonates.

The gangue carbonates of willemitic ore have compositions of $\delta^{18}O$ = +20.24‰ to +17.43‰ and $\delta^{13}C$ = +0.86‰ to +0.29‰. These values are close to hydrothermally altered metadolomites and hydrothermal carbonates of veins and breccias (Fig. 10) and represent the same covariance trend. This suggests a genetic link between the hydraulic brecciation, vein infilling, and willemitic mineralization.

Oxygen Isotopes in Willemitic Assemblage

The oxygen isotope analyses of willemite, franklinite, quartz, and hematite of the willemitic ore, are presented in Table 3. The observed ^{18}O partitioning is quartz > willemite > franklinite > hematite, which is similar to the partitioning of the willemite and the franklinite of Sterling Hill (Johnson et al., 1990). There are few other studies on the isotopic characteristics of these mineral phases. However, theoretical calculations of the temperature dependence of equilibrium oxygen isotope fractionation in minerals of zinc ore (Zheng, 1996) are useful for geothermometric studies, as discussed below.

Geothermometry

The geothermometric calculations were done using cogenetic mineral pairs from different associations, such as sulfide bodies (sphalerite-galena), willemitic ore (willemite-quartz, hematite-quartz) and hydrothermal phases of veins and breccia (siderite-quartz). These mineral pairs were chosen from petrographic studies, which indicate the relative chronology of mineral formation and equilibrium textures. The lack of reversals and the agreement of temperatures obtained by different stable isotope (O, C, S) and mineral chemistry geothermometers were utilized as an indication of isotopic equilibrium.

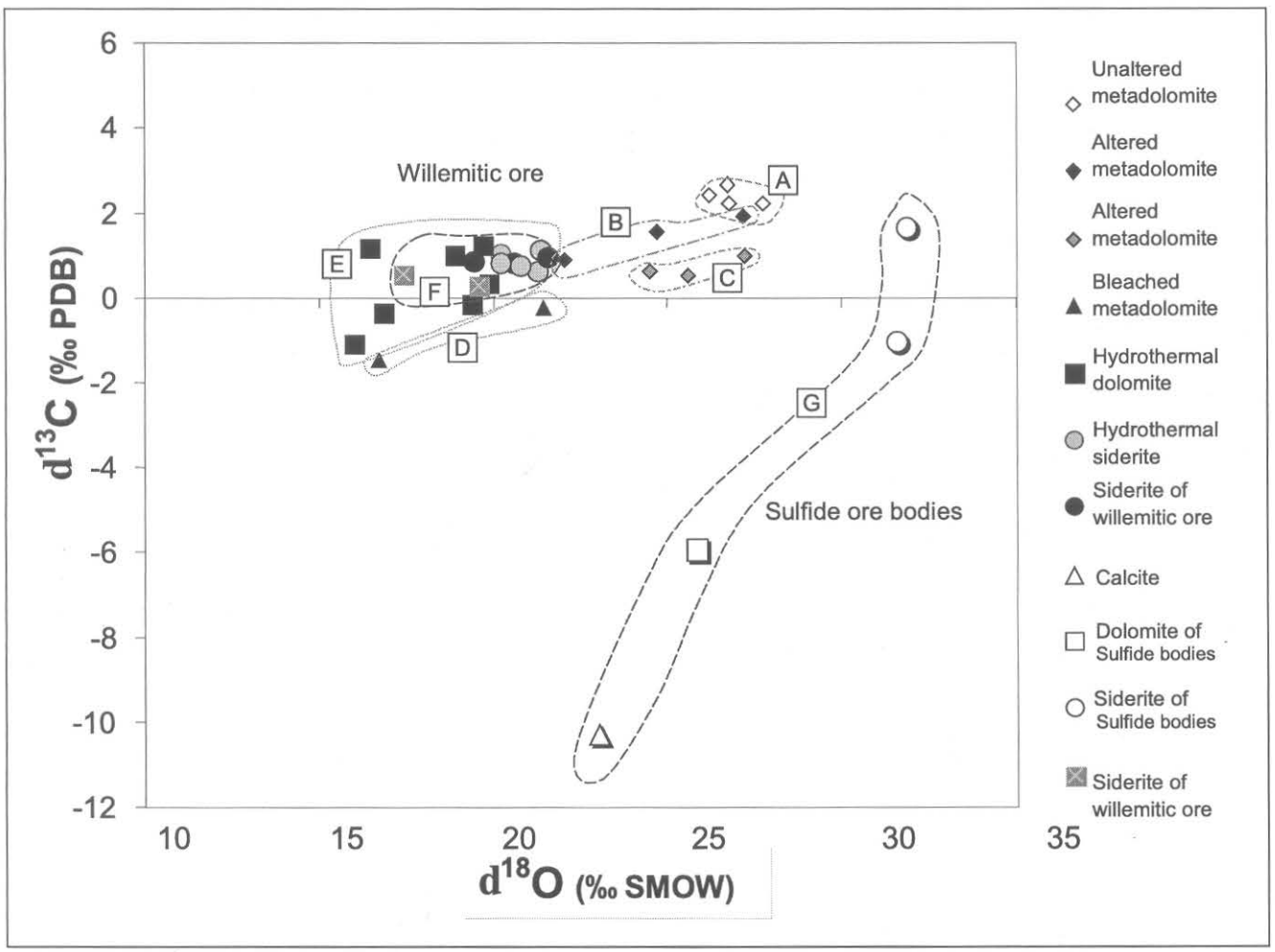

Fig. 10. The $d^{18}O$ vs $d^{13}C$ plots for carbonates from Vazante mine. A — unaltered metadolomites of Pamplona and Morro do Pinheiro members. B — hydrothermally altered metadolomite of Pamplona member. C — hydrothermally altered metadolomite of Morro do Pinheiro member. D — bleached metadolomite. E — dolomite and siderite from net veined breccias and willemitic ore. F — gangue carbonates (dolomite and siderite) from willemitic ore. G — gangue carbonates (dolomite and siderite) from sulfide orebodies.

Table 5. Calculated temperatures of mineral formation based on fractionation factors between mineral pairs and Cd distribution coefficient between galena and sphalerite

Amostras	Mineral	Reference	Calibration	T (°C)
Sulfide Orebodies				
Cogenetic mineral pairs related to britle-ductile structures				
VZ-01/VZ-29c	sp-ga	Sakai (1968)	Graphical method	330
VZ-01/VZ-29c	sp-ga	Kiyosu (1973)	$10^3 \ln\alpha = 8.91\ (10^5/T^2)$	312
VZ-01/VZ-29c	sp-ga	Kajiwara and Krouse (1971)	$10^3 \ln\alpha = 0.8\ (10^6/T^2)$	282
VZ-01/VZ-29c	sp-ga	Czamaske and Rye (1974)	$10^3 \ln\alpha = 0.7\ (10^6/T^2)$	246
VZ-01/VZ-29c	sp-ga	Rye (1974)	$10^3 \ln\alpha = 0.7\ (10^6/T^2)$	246
VZ-29g-C1	sp-ga	Geletii et al. (1979)	$\ln KD_{CdS} = 1.663 - [26.4\ (P\text{-}1)\ ]/T - 0.702$	317
Cogenetic mineral pairs related to britle structures				
VZ-29g-C3	sp-ga	Geletii et al. (1979)	$\ln KD_{CdS} = 1.663 - [26.4\ (P\text{-}1)\ ]/T - 0.702$	127
VZ-30-C1	sp-ga	Geletii et al. (1979)	$\ln KD_{CdS} = 1.663 - [(26.4\ (P\text{-}1)\ ]/T - 0.702$	110
Willemitic Ore				
VZ-29g	qtz-will	Zheng (1993)	$10^3 \ln\alpha = 0.69 \times 10^6/T^2 + 4.18 \times 10^3/T - 1.75$	294
VZ-29g/F-551-28	qtz-hm	Zheng (1991)	$10^3 \ln\alpha = 1.55 \times 10^6/T^2 + 9.05 \times 10^3/T - 482$	254
F-551-19/F-551-30	qtz-will	Zheng (1993)	$10^3 \ln\alpha = 0.69 \times 10^6/T^2 + 4.18 \times 10^3/T - 1.75$	263
F-551-19/F-551-30	qtz-hm	Zheng (1991)	$10^3 \ln\alpha = 1.55 \times 10^6/T^2 + 9.05 \times 10^3/T - 4.82$	206
F-551-19/F-551-26	qtz-sid	Becker and Clayton (1976)	Graphical method	261

Table 6. Fractionation factors between mineral-H_2O used in the oxygen isotope compositions of ore fluids calculation

Reference		Isotopic Fractionation Factor ($\ln 10^3\alpha_{min}$-H_2O)
Carbonates		
Northrop and Clayton (1966)	Δdol-H_2O	$3.20\ (10^6/T^2) - 2.00$
O'Neil et al.(1969)	Δcc-H_2O	$2.78\ (10^6/T^2) - 3.38$
Carothers et al. (1988)	Δsid-H_2O	$3.13\ (10^6/T^2) - 3.50$
Oxides and Silicates		
Clayton et al. (1972)	Δqtz-H_2O	$3.38\ (10^6/T^2) - 3.4$
Zheng (1991)	Δhm-H_2O	$2.69 \times 10^6/T^2 - 12.82 \times 10^3/T + 3.78$
Zheng (1993)	Δwill-H_2O	$3.79 \times 10^6/T^2 - 8.94 \times 10^3/T + 2.50$
Zheng (1996)	Δfrank1-H_2O	$2.88 \times 10^6/T^2 - 11.37 \times 10^3/T + 2.89$
Zheng (1996)	Δfrank2-H_2O	$2.52 \times 10^6/T^2 - 12.02 \times 10^3/T + 2.99$

Abreviations: dol = dolomite, sid = siderite, qtz = quartz, hm = hematite, will = willemite, frank1 = franklinite with spinel inverse structure, frank2 = spinel structure franklinite.

The data presented in Table 5 demonstrate distinct temperatures for sulfide related to ductile-brittle structures in stratabound mineralization (317°C) and to brittle features (110°C to 127°C). The estimated temperatures of willemitic mineralization related to ductile-brittle structures vary from 206°C to 294°C (Table 5), and are similar to those estimated for sulfides controlled by these structures.

Fluid Evolution

The oxygen isotopic compositions of the fluids in equilibrium with hydrothermal minerals were estimated by applying the isotopic compositions of minerals, the temperature interval calculated by geothermometric studies, and the fractionation factor between mineral-H_2O (Table 6). The results imply uncertainty in relation to the fluid reservoir due to the possibility of a similar isotopic composition that could be compatible with different types of fluids, multiples sources and isotopic exchanges due to fluid-rock interaction processes.

The calculated isotopic compositions of fluids in equilibrium with minerals of the vein systems, such as dolomite, siderite, hematite, quartz, ($\delta^{18}O$ = +11.05‰) and with gangue and willemitic ore, such as dolomite, siderite, hematite, quartz, willemite ($\delta^{18}O$ = +11.81‰), at 250°C, are similar (Fig. 11), suggesting that the hydraulic brecciation, vein infilling, and willemitic ore could be associated with the same hydrothermal fluid. However, the $\delta^{18}O$ of gangue minerals of the sulfide mineralization (siderite, dolomite, franklinite), for the same temperature (250°C), indicates that the fluids responsible for those minerals were strongly enriched in ^{18}O, with an average $\delta^{18}O$ composition of +19.4‰ (Fig. 11).

These calculated isotopic compositions of the hydrothermal fluids should reflect final compositions, due to interaction processes, such as, fluid-rock exchange, fluid mixing and secondary fluid percolation. These processes generally result in values more enriched in $\delta^{18}O$ than original fluids. According to Zheng and Hoefs (1993), the covariance trends of $\delta^{18}O$ and $\delta^{13}C$ of carbonates may inform us about the processes related to fluid evolution, which can be investigated through quantitative models. Thus, the models of fluid/rock interaction and fluid mixing (Zheng and Hoefs, 1993) were used for hydrothermal dolomite related to sulfide and willemitic mineralization, based on the fractionation factors of the oxygen isotope of Northrop and Clayton (1966) (dolomite-H_2O) and of the carbon isotope of Ohmoto and Rye (1979) (dolomite-H_2CO_3).

The fractionation factor between carbonate-H_2CO_3 was used considering that oxidized species of carbon (H_2CO_3

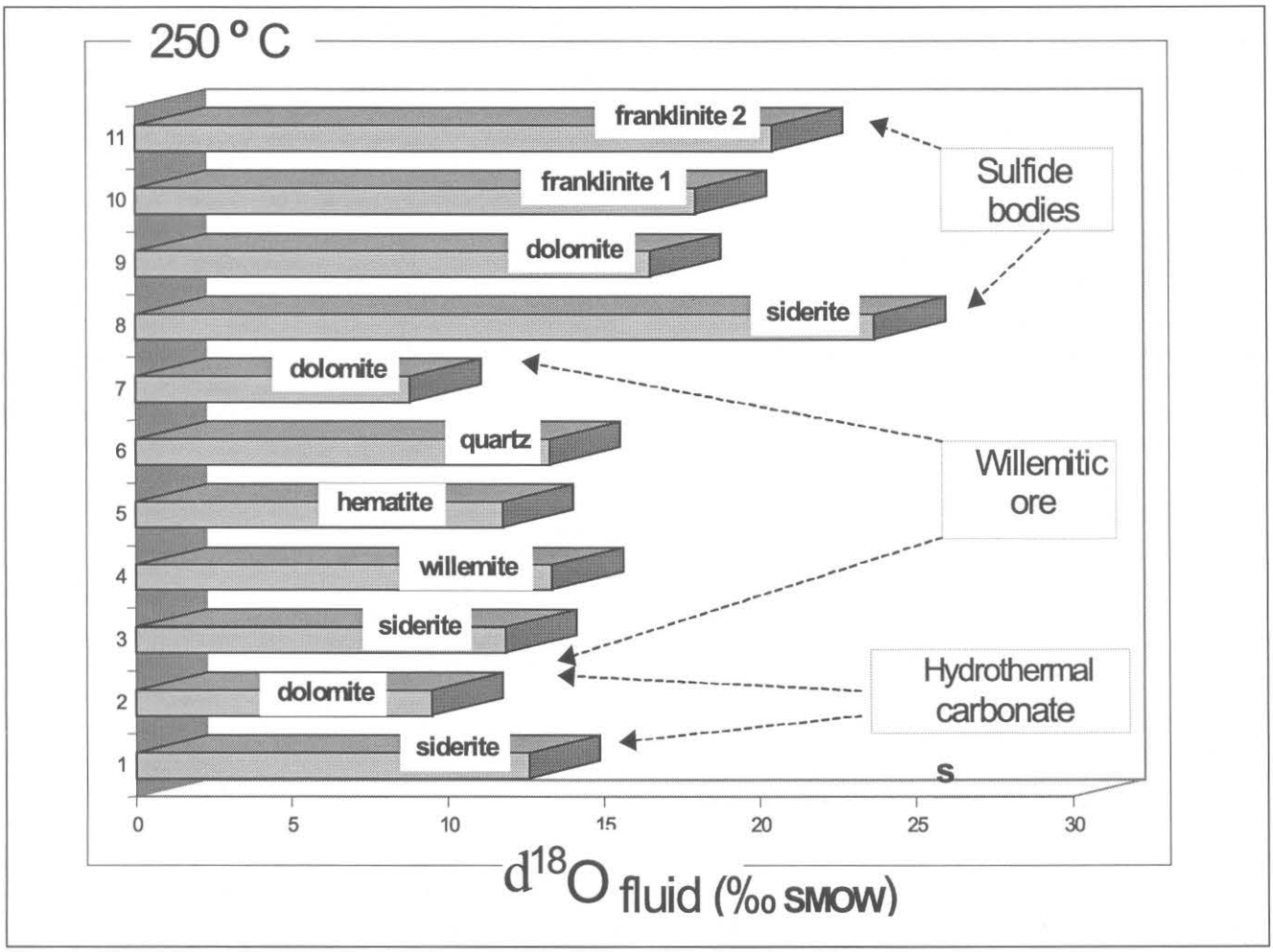

Fig. 11. Calculated oxygen isotope compositions of hydrothermal fluids responsible for the Vazante mineralization, based on fractionation factors between mineral and water (see Table 4) at 250°C.

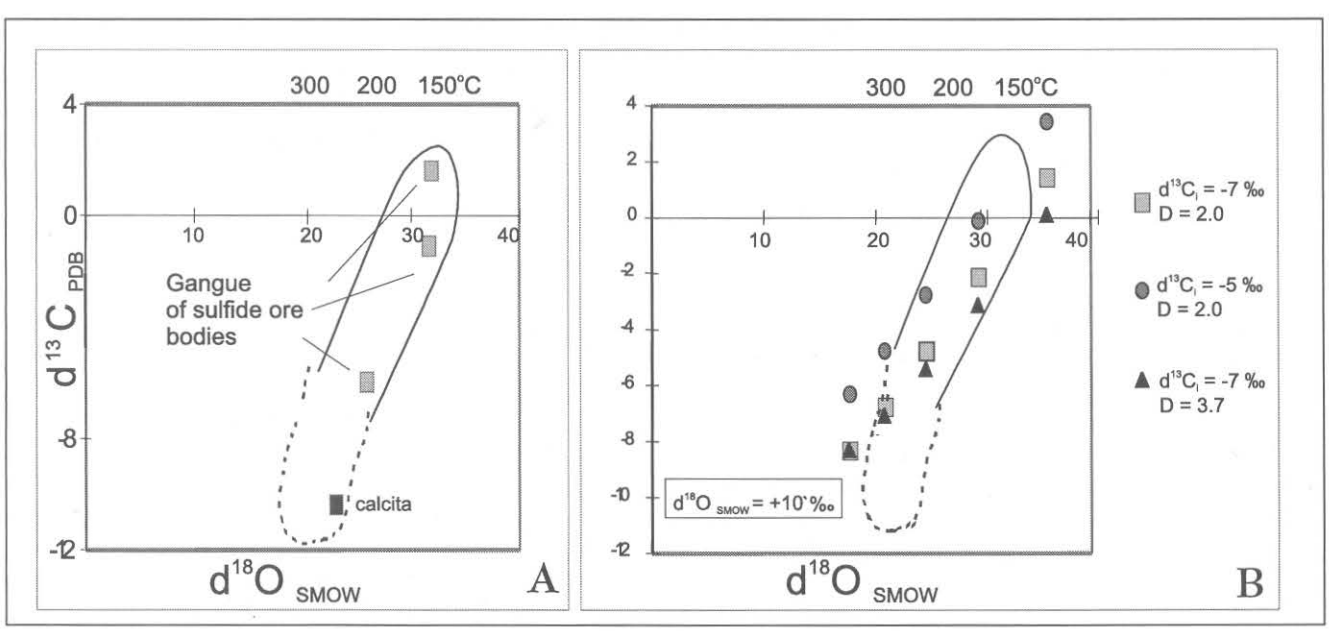

Fig. 12. Covariation plots between $d^{18}O$ and $d^{13}C$ values of carbonates. A — calculated oxygen and carbon isotope compositions for carbonates, formed by a hydrothermal fluid with $d^{18}O = +10‰$ and different values of $d^{13}C$, based on fluid-rock interaction model of Zheng and Hoefs (1993). B — covariation plots between $d^{18}O$ and $d^{13}C$ values of carbonates related to sulfide orebodies of the Vazante deposit.

and HCO_3^-) are dominant in the fluid due to high fO_2 inferred by mineral stability fields. The small difference between the isotopic composition of these species (≈ 0.11‰), as estimated by Ohmoto (1972) and Ohmoto and Rye (1979), was also considered.

Sulfide Mineralization from Fluid-rock Interaction

The fluid-rock interaction model (Zheng and Hoefs, 1993) is probably the most appropriate to constrain the isotopic signature of gangue carbonates associated with sulfide mineralization. The isotopic compositions of the hydrothermal carbonate can be given by the equation:

$$\delta^{13}C = \delta^{13}C^i \text{ fluid} + 10^3 \ln\alpha_{\text{carbonate-fluid}} + R/W \bullet \Delta^{13}C^i_f$$

$$\delta^{18}O = \delta^{18}O^i \text{ fluid} + 10^3 \ln\alpha_{\text{carbonate-}H_2O} + R/W \bullet \Delta^{18}C^i_f$$

where $\Delta^{13}C^i_f = \delta^i_{\text{rock}} - \delta^f_{\text{rock}}$, R/W = rock/water ratio,

where known isotopic compositions of unaltered and altered host rocks are used for ΔC^i_f calculations. The assumed initial temperature of the hot hydrothermal fluid is about 300°C, which is compatible with geothermometric studies (see above). A progressive decrease of temperature associated with variations in the material-balance R/W ratio, in the range of 0.1 to 1, was also considered.

The above model was applied for a large interval of hydrothermal fluid composition ($\delta^{13}C^i_{\text{fluid}}$ and $\delta^{18}O^i_{\text{fluid}}$), which represents all known fluid reservoirs. In this way, the original isotopic composition of hydrothermal fluid of $\delta^{18}O$ = +10‰ and $\delta^{13}C$ = -7‰ (Fig. 12) fits the model better and could match the gangue carbonate isotopic compositions. However, this composition would be compatible with different reservoirs, such as connate, magmatic or metamorphic sources.

The isotopic composition of magmatic fluids vary between $\delta^{18}O$ = +5.5‰ to +10‰ (Taylor, 1979) and the exsolved CO_2 present in this fluid type has $\delta^{13}C$ composition between -3.5‰ to -7‰ (Zheng and Hoefs, 1993). ^{13}C depleted calcite occurs only in metadolomites in contact with metabasites, which could indicate an igneous source of carbon. However, the ^{12}C contribution of the small metabasic bodies to the hydrothermal system and their implications in the formation of sulfide bodies cannot be estimated.

A metamorphic origin associated with liberation of volatile constituents of the host sequence could have mixed characteristics, with both sedimentary and igneous similarities. This origin could be responsible for a local contribution of depleted carbon from metabasites as well. The main sulfide

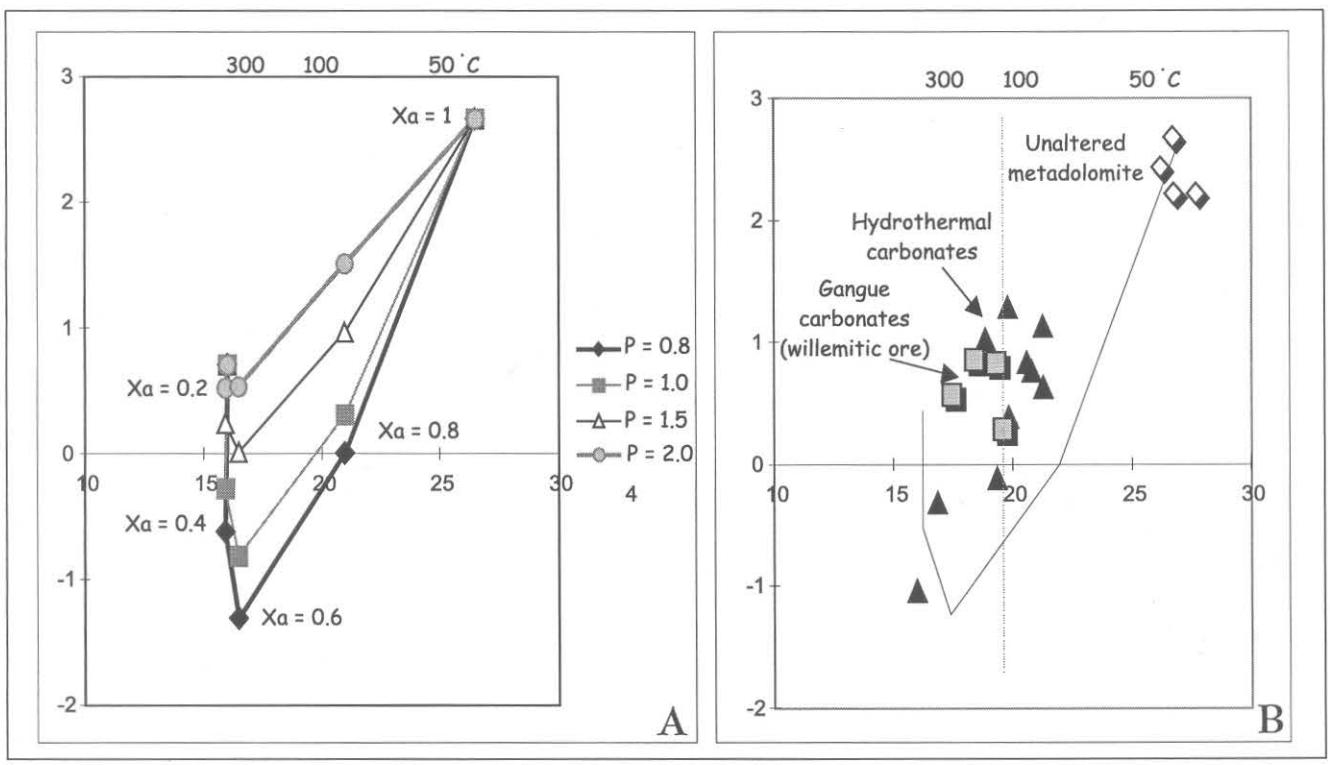

Fig. 13. Covariation plots between $d^{18}O$ and $d^{13}C$ values of carbonates. A — calculated oxygen and carbon isotope compositions for carbonates derived from mixture of two types of fluid, based on Zheng and Hoefs (1993) model. The end-member compositions of both evolved fluids are of $d^{18}O$ = 0‰ and $d^{13}C$ = -7‰, and of $d^{18}O$ = +10‰ and $d^{13}C$ = +2‰ respectively. The first fluid has a low temperature of 50°C, whereas the second has a high temperature of 300°C. X_a is the mole fraction of the first fluid in the mixed solution and P is the concentration ratio of total dissolved carbon in fluid B to in fluid A. Different oxygen and carbon isotope compositions for carbonate result of different proportions of the two fluids and P values. B — relationship between $d^{18}O$ and $d^{13}C$ values of gangue and hydrothermal carbonates related to willemitic ore and the representative mixing curve of calculated oxygen and carbon compositions of carbonates derived from fluid mixture with P = 0.8.

and carbonate precipitation mechanism is probably related to temperature decrease and the positive correlation of $\delta^{18}O$ and $\delta^{13}C$ could be associated with CO_2 degassing, produced by progressive temperature changes during fluid-rock interaction.

Willemitic Ore from a Mixture of Different Fluids

The observed characteristics of gangue carbonates related to willemitic ore could reflect fluid mixture within the shear zone. Using the Zheng and Hoefs (1993) model, the hydrothermal carbonates formed by interaction of two distinct fluids (A and B) present the following isotopic compositions:

$$\delta^{13}C_{carbonate} = X_A\,(\delta^{13}C_A + 10^3\ln\alpha_{carbonate\text{-}fluid}) + P\,(1 - X_A)(\delta^{13}C_B + 10^3\ln\alpha_{carbonate\text{-}fluid})/P + X_A - PX_A$$

$$\delta^{18}O_{carbonate} = \delta^{18}O_B + 10^3\ln\alpha_{carbonate\text{-}H_2O} + X_A\,(\delta^{18}O_A - \delta^{18}O_B),$$

where X_A represents the molar fraction of fluid A in the mixture and $P = ({}^{12}C_B/{}^{12}C_A)$.

A mixture of a fluid A, having composition of $\delta^{18}O$ = 0‰ and $\delta^{13}C$ = -7‰ and a temperature of 50°C, with a hot hydrothermal fluid B having $\delta^{18}O$ = +10‰ and $\delta^{13}C$ = +2‰ and a temperature of 300°C, was considered. The chosen values of P are between 0.8 and 2.0.

Through calculation, we obtained, from fluid A, a composition of $\delta^{18}O$ = +26.6‰ and $\delta^{13}C$ = +2.66‰, close to that of unaltered host rocks ($\delta^{18}O$ = +26.6‰ and $\delta^{13}C$ = +2.22‰). From this, we conclude that for temperature (50°C), the isotopic exchanges are slow and the isotopic compositions are not significantly altered.

The distribution of Vazante hydrothermal carbonates in the $\delta^{18}O$-$\delta^{13}C$ space coincide with the compositions obtained for a temperature interval of 100°C to 300°C, with P between 1 and 2, and a fluid mixture of X_A= 0.8 and X_B = 0.2 (Fig. 13).

The gangue carbonates of willemitic ore would be in equilibrium with higher proportions of fluid B, and consequently, high temperatures, which is consistent with our geothermometric data (260°C to 294°C).

The isotopic composition of fluid A could be related to meteoric fluids, which, according to Taylor (1987) has $\delta^{18}O$ near to 0‰ and can display negative values of $\delta^{13}C$ (up to -7‰) associated with dissolved atmospheric CO_2. This meteoric fluid could introduce SiO_2, Fe_2O_3, As, Sb, V, W, and LREE in the system and favor the formation of willemite ore.

The isotopic composition of fluid B would be similar, mainly in $\delta^{18}O$ values, to fluids involved with the carbonate gangue of sulfide bodies. Thus, the mixture of meteoric and metamorphic fluids, linked to shear-zone development, could result in hydraulic brecciation and willemitic mineralization, related to physico-chemical modification of the fluids, such as an increase in fO_2, consistent with stability fields of the observed mineral assemblage.

Conclusions

Within the Vazante Shear Zone, the conditions for sulfide and willemite formation are similar. The majority of the ore deposition occurred at temperatures that range from 200°C to 300°C. This temperature interval reflects the prevalent metamorphic conditions at the time of the shear zone development. The willemitic assemblage had to occur at narrow intervals of high fO_2.

The sulfides are related to metalliferous fluid of metamorphic origin, which is, also, responsible for mobilizing and concentrating Zn, Pb, and Cd. The likely source for the metals in these deposits is the sedimentary basin itself. The $\delta^{34}S$ ratios of sulfides indicate a direct crustal origin for the sulfur, which was transported by a metamorphic fluid. This favors their origin being from pre-existing sulfide orebodies or from thermochemical sulfate reduction and hydrothermal transport.

The occurrence in the Vazante-Unaí region of diagenetic deposits, such as Morro Agudo (Misi et al., 1996 and Freitas-Silva and Dardenne, 1997), could be related to a hydrothermal paleo-system, allowing discharge of metalliferous brines under euxinic conditions. Anoxic conditions would be a key controlling factor for the formation and preservation of sulfide-dominant deposits in the Vazante-Unaí region. However, there is no evidence of prevalent anoxic conditions within the Pamplona member, host of the Vazante deposit. Instead, the hydrothermal discharge of metalliferous brines under different oxidation states may have generated mineral phases, which reflect high fO_2. This explains the lack of iron sulfides in the Vazante mine, a situation similar to the metalliferous sediments of the Red Sea and to the protholith of the Sterling Hill ore deposit, U.S.A. (Johnson et al., 1990).

Some genetic aspects of the willemitic ore might be better explained by the interplay of various factors, such as, specific physico-chemical conditions and a coeval local stress regime, responsible for the Vazante Shear Zone. These conditions would permit the interaction and mixing of metalliferous metamorphic and SiO_2-bearing meteoric fluids.

Acknowledgment

This paper is part of a M.Sc. dissertation of the first author on the Vazante zinc mine.

The authors are grateful to Companhia Mineira de Metais for continuous support and hospitality at the mine and permission to publish. Special thanks are due to Natural Environment Research Council, Isotope Geosciences Laboratory, for access to its stable isotope analytical facilities and to Peter Greenwood, Melanie Leng and Hillary Sloane with whom the isotope studies were conducted.

The manuscript benefited from constructive comments by Alex Brown and one anonymous reviewer, to whom we are indebted.

The financial support was provided by Fundo de Amparo à Pesquisa do Estado de São Paulo, Brasil

(Research Grant No. 96/3941-3 and 98/0412-5 to J.S. Bettencourt) which we acknowledge with appreciation.

References

ALMEIDA, F.F.M de, 1967. Origem e evolução da plataforma brasileira. Boletim DNPM, 243, 36 p.

ALMEIDA, F.F.M. de, 1993. Limites do Cráton do São Francisco em Minas Gerais-Síntese dos conhecimentos. II Simpósio do Cráton do São Francisco, p. 256-259.

AMARAL, G., 1966. Isótopos de chumbo e gênese das jazidas de Vazante e Itacarambi Publicação 01. Sociedade Brasileira de Geologia-Núcleo Rio de Janeiro, p. 45.

AMARAL, G., 1968. Geologia e Depósitos de Minério na Região de Vazante, Estado de Minas Gerais. Ph.D. thesis, Universidade de São Paulo, 133 p.

AMARAL, G. and KAWASHITA, K., 1967. Determinação da idade do Grupo Bambuí pelo método Rb/Sr. Proceedings, XXI Congresso Brasileiro de Geologia. Anais, Sociedade Brasileira de Geologia, p. 214-217.

BABINSKI, M., 1993. Idades isocrônicas Pb/Pb e geoquímica isotópica de Pb das rochas carbonárticas do Grupo Bambuí na porção Sul da Bacia do São Francisco. Ph.D. thesis, Instituto de Pesquisas Energéticas e Nucleares, 133 p.

BECKER, R.H. and CLAYTON, R.N., 1976. Oxygen isotope study of a Precambrian banded iron formation, Hamersley Range, Western Australia. Geochimica et Cosmochimica Acta, 40, p. 1153-1165.

BORTHWICK, J. and HARMON, R.S., 1982. A note regarding Cl_3 as an alternative to BrF_5 for oxygen isotope analysis. Geochimica et Cosmochimica Acta, 46, p. 1665-1668.

BOSTRÖM, K., 1973. The origin and fate of ferromanganoan active ridge sediments. Stockholm Contributions to Geology, 27, p. 147-243.

CAROTHERS, W.W., ADAMI, L.H. and ROSENBAUER, R.J., 1988. Experimental oxygen isotope fractionation between siderite-water and phosphoric acid liberated CO_2-siderite. Geochimica et Cosmochimica Acta, 52, p. 2445-2450.

CASSEDANNE, J. and LASSERRE, M., 1969. Análise isotópica pelo método do chumbo em algumas galenas brasileiras: Descrição do método utilizado. Mineração e Metalurgia, XLIX, p. 215-224.

CHANG, H.K., KAWASHITA, K., ALKMIM, F.F. and MOREIRA, M.Z., 1993. Considerações sobre a estratigrafia e evolução tectônica da Bacia do São Francisco. *In* Proceedings, Congresso Brasileiro de Geologia, 35. Sociedade Brasileira de Geologia, 5, p. 2076-2090.

CLAYTON, R.N. and MAYEDA, T.K., 1963. The use of bromine pentafluoride in the extraction of oxygen from oxides and silicates for isotopic analysis. Geochimica et Cosmochimica Acta, 27, p. 43-52.

CLAYTON, R.N, O'NEIL, J.R. and MAYEDA, T.K., 1972. Oxygen isotope exchange between quartz and water. Journal of Geophysical Research, 77, p. 3057-3067.

CLOUD, P.E. and DARDENNE, M.A., 1973. Proterozoic age of the Bambuí Groupe in Brazil. Geological Society of America Bulletin, 84, p. 1673-1676.

COUTO, J.G.P., CORDANI, U.G., KAWASHITA, K., IYER, S.S. and MORAES, N.M.P., 1981. Considerações sobre a idade do Grupo Bambuí com base em análises isotópicas de Sr e Pb. Revista Brasileira de Geociências, 11, p. 5-16.

CUMMING, G.L. and RICHARDS, J.R., 1975. Ore lead isotope relations in a continuously changing earth. Earth and Planetary Science Letters, 28, p. 155-171.

CZAMASKE, G.K. and RYE, R.O., 1974. Experimentally determined sulfur isotope fractionations between sphalerite and galena in temperature range 600°C to 275°C. Economic Geology, 69, p. 17-25.

DA ROCHA ARAÚJO, P.R., FLICOTEAUX, R., PARRON, C. and TROMPETTE, R., 1992. Phosphorites of Rocinha Mine, Patos de Minas, Minas Gerais, Brazil: Genesis and evolution of a Middle Proterozoic deposit tectonized by the Brasiliano Orogeny. Economic Geology, 87, p. 332-351.

DARDENNE, M.A., 1978. Síntese sobre a estratigrafia do Grupo Bambuí no Brasil Central. *In* Proceedings, XXX Congresso Brasileiro de Geologia. Sociedade Brasileira de Geologia, 2, p. 597-610.

DARDENNE, M.A., 1979. Les minéralisations plomb-zinc du Groupe Bambui et leur contexte géologique. Ph.D. thesis, Université Pierre et Marie Curie, Paris VI, 275 p.

DARDENNE, M.A. and FREITAS-SILVA, F.H., 1998. Depósitos Pb-Zn-F-Ba do Supergrupo São Francisco. *In* Proceedings, XL Congresso Brasileiro de Geologia. Sociedade Brasileira de Geologia, p. 133.

DOE, B.R. and ZARTMAN, R.E., 1979. Plumbotectonics I, the Phanerozoic. *In* Geochemistry of Hydrothermal Ore Deposits. *Edited by* H.L. Barnes. John Wiley & Sons, New York, p. 22-70.

DONNELLY, T.H. and CRICK, I., 1992. Biological and abiological sulfate reduction in two northern Australian Proterozoic basins. *In* Early Organic Evolution: Implications for Mineral and Energy Resources. *Edited by* M. Schidlowski, S. Golubic, M.M. Kimberley, D.M. McKirdy, and P.A. Trudinger. Springer-Verlag, Berlin, Heidelberg.

ESSENE, E.J. and PEACOR, D.R., 1987. Petedunnite ($CaZnSi_2O_6$), a new clinopyroxene from Franklin, New Jersey, and phase equilibria for zincian pyroxenes. American Mineralogist, 72, p. 157-166.

FIELD, C.W. and FIFAREK, R.H., 1985. Light stable-isotope systematics in the epithermal environment. *In* Geology and Geochemistry of Epithermal Systems. *Edited by* B.R. Berger and P.M. Bethke. Reviews in Economic Geology, 2, p. 99-128.

FREITAS-SILVA, F.H., 1996. Metalogênese do Depósito do Morro Ouro, Paracatú, MG. Ph.D. thesis, University of Brasília, 338 p.

FREITAS-SILVA, F.H. and DARDENNE, M.A., 1997. Pb/Pb isotopic patterns of galenas from Morro do Ouro (Paracatu Formation), Morro Agudo/Vazante (Vazante Formation) and Bambuí Group deposits. South-American Symposium on Isotope Geology, Extended Abstracts, p. 118-120.

FRONDEL, C. and BAUM, J.L., 1974. Structure and mineralogy of the Franklin zinc-iron-manganese deposit, New Jersey. Economic Geology, 69, p. 157-180.

FUCK, R.A., 1994. A Faixa Brasília e a campartimentação tectônica na Província Tocantins. *In* Proceedings, IV Simpósio de Geologia do Centro-Oeste. Sociedade Brasileira de Geologia, p. 184-187.

FUCK, R.A, JARDIM DeSá, E.F., PIMENTEL, M.M., DARDENNE, M.A. and PEDROSA SOARES, A.C., 1993. As faixas de dobramentos marginais do Cráton do São Francisco: Síntese dos conhecimentos. *In* Proceedings, O Cráton do São Francisco. *Edited by* J.M.L. Dominguez and A. Misi. Sociedade Brasileira de Geologia/Superintendência de Geologia e Recursos Minerais, p. 161-186.

GELETII, V.F., CHEENISHEV, L.V. and PASTUSHKOVA, T.M., 1979. Distribution of cadmium and manganese between galena and sphalerite. Geologiia Rudnykv Mestorozhdenii, 21, p. 66-75.

HITZMAN, M.W., THORMAN, C.H., ROMAGNA, G., OLIVEIRA, T.F. and DARDENNE, M.A., 1995. The Morro Agudo Zn-Pb deposit, Minas Gerais, Brazil: A Proterozoic Irish-type carbonate hosted sedex replacement deposit. Geological Society of America, Abstracts with Programs, 27, p. A408.

HOLMES, A., 1946. Na estimate of the age of the earth. Nature, 157, p. 680.

HOUTERMANS, F.G., 1946. The isotope ratios in natural lead and the age of uranium. Naturwissenschaften, 33, p. 185.

IYER, S.S., 1984. A discussion on the lead isotope geochemistry of galenas from the Bambuí Group, Minas Gerais, Brazil. Mineralium Deposita, 19, p. 132-137.

IYER, S.S, HOEFS, J. and KROUSE, H.R., 1992. Sulfur and lead isotope geochemistry of galenas from Bambuí Group, Minas Gerais, Brazil: Implications on ore genesis. Economic Geology, 87, p. 437-443.

IYER, S.S., KROUSE, H.P. and BABINSKI, M., 1993. Isotope investigations on carbonate rocks hosted lead-zinc deposits from Bambuí Group, Minas Gerais, Brazil: Implications for ore genesis and prospect evaluation. *In* Proceedings, II Simpósio do Cráton do São Francisco. Sociedade Brasileira de Geologia/Superintendência de Geologia e Recursos Minerais, p. 338-339.

JOHNSON, C.A., RYE, D.M. and SKINNER, B.J., 1990. Petrology and stable isotope geochemistry of the metamorphosed zinc-iron-manganese deposit at Sterling Hill, New Jersey. Economic Geology, 85, p. 1133-1161.

KAJIWARA, Y. and KROUSE, H.R., 1971. Sulfur isotope partitioning in metallic sulfide systems. Canadian Journal of Earth Sciences, 8, p. 1397-1408.

KAWASHITA, K., MIZUSAKI, A.M.P. and CHANG, H.K., 1987. Razões $^{87}Sr/^{86}Sr$ em sedimentos carbonáticos do Grupo Bambuí (MG). *In* Proceedings, I Congresso Brasileiro de Geoquímica. Sociedade Brasileira de Geoquímica, 1, p. 133-137.

KAWASHITA, K., THOMAZ FILHO, A., SATO, K., KAWASHITA, M.Y. and BABINSKI, M., 1993. Idade do Grupo Bambuí (MG) com base em isótopos de Carbono, Oxigênio, Estrôncio e Enxofre. *In* Proceedings, II Congresso de Geoquímica dos Países de Língua Portuguesa. Universidade do Porto, Memórias 3, p. 391.

KIYOSU, Y., 1973. Sulfur isotopic fractionations among sphalerite, galena and sulfide ions. Geochemical Journal, 7, p. 191-199.

LAZNICKA, P., 1989. Breccias and ores. Part 1: History, organization and petrography of breccias. Ore Geology Rewiews, 4, p. 315-344.

MARCHESE, H.G., 1974. Estromatolitos *Gymnosolenidos* en el lado oriental de Minas Gerais, Brasil. Revista Brasileira de Geociências, 4, p. 257-271.

MARINI, O.J., FUCK, R.A, DANNI, J.C. and DARDENNE, M.A., 1981. A evolução geotectônica da Faixa Brasília e de seu embasamento. *In* Proceedings, Simpósio sobre o Cráton do São Francisco e suas Faixas Marginais. Companhia de Pesquisa de Recursos Minerais/Sociedade Brasileira de Geologia, p. 100-115.

McCREA, J.M., 1950. On the isotope chemistry of carbonates and paleotemperature scale. Journal of Chemical Physics, 18, p. 849-857.

MISI, A., IYER, S.S. and TASSINARI, C.C.G., 1996. Boquira (2.5 Ga) and Morro Agudo (0.65 Ga) lead-zinc deposits, Brazil: New SEDEX subtypes? *In* Proceedings, XXXIX Congresso Brasileiro de Geologia. IGCP Project 342: Age and Isotopes of South American Ores, p. 251-253.

MISI, A., TASSINARI, C.C.G. and IYER, S.S., 1997. New isotope data from the Proterozoic lead-zinc (Ag) sediment-hosted sulfide deposits of Brazil: Implications for their metallogenic evolution. South-American Symposium on Isotope Geology, Extended Abstracts, p. 201-203.

MOERI, E., 1972. On a columnar stromatolite in the Precambrian Bambuí Group of Central Brazil. Eclogae Geologicae Helvetiae, 65, p. 185-195.

MONTEIRO, L.V.S., 1997. Contribuição à gênese das mineralizações de Zn e Pb da Mina Vazante (MG). Master dissertation, University of São Paulo, 159 p.

MONTEIRO, L.V.S., BETTENCOURT, J.S. and GRAÇA, R., 1996. Contribuição à gênese das mineralizações de Zn e Pb da Mina Vazante (MG): Um estudo preliminar. *In* Proceedings, XXXIX Congresso Brasileiro de Geologia. Sociedade Brasileira de Geologia, 5, p. 501-503.

NORTHROP, D.A. and CLAYTON, R.N., 1966. Oxygen isotope fractionations in systems containing dolomite. Journal of Geology, 74, p. 174-195.

OHMOTO, H., 1972. Systematics of sulfur and carbon isotopes in hydrothermal ore petrology. Economic Geology, 67, p. 552- 579.

OHMOTO, H., 1986. Stable isotope geochemistry of ore deposits. *In* Stable Isotopes in High Temperature Geological Processes. *Edited by* J.W. Valley, H.P. Taylor, Jr. and J.R. O'Neil. Mineralogical Society of America, Reviews in Mineralogy, 16, p. 491-560.

OHMOTO, H., 1996. Formation of volcanogenic massive sulfide deposits: The Kuroko perspective. *In* The Conjunction of Processes Resulting in the Formation of Orebodies. *Edited by* R.M. Veielreicher, D.I. Groves, C.A. Heinrich, and J.L. Washe. Ore Geology Reviews, 10, p. 135-178.

OHMOTO, H. and RYE, R.O., 1979. Isotopes of sulfur and carbon. *In* Geochemistry of Hydrothermal Ore Deposits, 2nd edition. *Edited by* H.L. Barnes. John Wiley and Sons, New York, p. 509-567.

O'NEIL, J.R, CLAYTON, R.N. and MAYEDA, T.K., 1969. The oxygen isotope fractionation in divalent metal carbonates. Journal of Chemical Physics, 51, p. 5547-5558.

PETER, J.M. and GOODFELLOW, W.D., 1996. Mineralogy, bulk and rare earth element geochemistry of massive sulfide-associated hydrothermal sediments of the Brunswick Horizon, Bathurst Mining Camp, New Brunswick. Canadian Journal of Earth Sciences, 33, p. 252-283.

PINHO, J.M.M., 1990. Evolução tectônica da mineralização de zinco de Vazante. Masters thesis, Universidade de Brasília, 130 p.

PINHO, J.M.M, DARDENNE, M.A. and RIGOBELLO, A.E., 1989. Evolução tectônica da mineralização de zinco de Vazante. *In* Proceedings, V Simpósio de Geologia do Núcleo Minas Gerais, 110, p. 275-276.

PINHO, J.M.M, DARDENNE, M.A. and RIGOBELLO, A.E., 1990. Caracterização da movimentação transcorrente da falha de Vazante, Vazante, MG. *In* Proceedings, XXXVI Congresso Brasileiro de Geologia. Sociedade Brasileira de Geologia, 5, p. 2284-2295.

RAFTER, T.A., 1965. Recent sulfur isotope measurements on a variety of speciman examined in New Zealand. Bulletin of Volcanology, 28, p. 3-20.

RIEDEL, W., 1929. Zur Mechanik geologisher Brucherscheinungen. Centralblatt für Mineralogie, Geologie, und Paleontologie, Part B: 354-368.

RIGOBELLO, A.E., BRANQUINHO, J.A., DANTAS, M.G. DA S., OLIVEIRA, T.F. and NEVES FILHO, W., 1988. Mina de Zinco de Vazante. *In* Principais depósitos minerais do Brasil. *Edited by* C. Shobbenhaus and C.E.S. Coelho. Departamento Nacional da Produção Mineral, 3, p. 101- 110.

RUSSEL, R.D. and FARQUHAR, R.M., 1960. Lead Isotopes in Geology. Interscience, New York, 243 p.

RYE, R.O., 1974. A comparison of sphalerite-galena sulfur isotope temperatures with filling temperatures of fluid inclusions. Economic Geology, 69, p. 26-32.

SAKAI, H., 1968. Isotopic properties of sulfur compounds in hydrothermal processes. Geochemical Journal, 2, p. 29-49.

SASAKI, A., ARIKAWA, Y. and FOLINSBEE, R.E., 1979. Kiba reagent method of sulfur extraction applied to isotope work. Bulletin of Geological Survey of Japan, 30, p. 241-245.

SCHOBBENHAUS, C., CAMPOS, D.A., DERZE, G.R. and ASMUS, H.E. (editors), 1981. Mapa Geológico do Brasil e da Área Oceânica adjacente, incluindo depósitos minerais (1:2500000). Brasília, Ministério das Minas e Energia/Departamento Nacional da Produção Mineral.

SIBLEY, D.F. and GREGG, J.M., 1987. Classification of dolomite rock textures. Journal of Sedimentary Petrology, 57, p. 967-975.

STACEY, J.C. and KRAMERS, J.D., 1975. Approximation of terrestrial lead isotope evolution by a two-model. Earth and Planetary Science Letters, 26 p. 207-221.

SWEENEY, M.A., PATTRICK, R.A.D. and VAUGHAN, D.J., 1991. The nature and genesis of the Willemite deposits of Zambia. *In* Source, Transport and Ore Deposition of Metals. *Edited by* M. Pagel and J. Leroy. Balkema, Rotterdam, p. 139-142.

TAYLOR, B.E., 1987. Stable geochemistry of ore-forming fluids. *In* Short Course, Stable Isotope Geochemistry of Low-temperature Fluids. Mineralogical Association of Canada, 13, p. 337-452.

TAYLOR, H.P., JR., 1979. Oxygen and hydrogen isotope relationships in hydrothermal mineral deposits. *In* Geochemistry of Hydrothermal Ore Deposits, 2nd edition. *Edited by* H.L. Barnes, John Wiley and Sons, New York, p. 336-377.

THOMAZ FILHO, A. and BONHOMME, M.G., 1979. Datations isotopiques Rb-Sr et K-Ar dans le Groupe Bambuí, à São Francisco (MG), au Brésil. Phase métamorphique brésilienne synchrone de la première phase panafricaine. Compte Rendu, Académie des Sciences, Paris, Series D, 198, p. 1221-1224.

THOMAZ FILHO, A. and LIMA, V.Q., 1981. Datação radiométrica de rochas sedimentares pelíticas pelo método Rb/Sr. Boletim Técnico Petrobrás, 24, p. 109-119.

VALENTE, C.R., 1993. A tectônica Transpressiva Proterozóica da Borda Ocidental do Craton do São Francisco. *In* Proceedings, II Simpósio do Cráton do São Francisco. Sociedade Brasileira de Geologia, p. 292-294.

ZARTMAN, R.E. and DOE, B.R., 1981. Plumbotectonic — The model. Tectonophysics, 75, p. 135-162.

ZHENG, Y-F., 1991. Calculation of oxygen isotope fractionation in metal oxides. Geochimica et Cosmochimica Acta, 55, p. 2299-2307.

ZHENG, Y-F., 1993. Calculation of oxygen isotope fractionation in anhydrous silicate minerals. Geochimica et Cosmochimica Acta, 57, p. 1079-1091.

ZHENG, Y-F., 1996. Oxygen isotope fractionation in zinc oxides and aplications for zinc mineralization in Sterling Hill deposit, USA. Mineralium Deposita, 31, p. 98-103.

ZHENG, Y-F and HOEFS, J., 1993. Theoretical modeling on mixing processes and application to Pb-Zn deposits in the Harz Mountains, Germany. Mineralium Deposita, 28, p. 79-89.